2019

SIMPLIFYING TECHNIQUES APPLIED TO COMPUTATIONAL FLUID DYNAMICS MODELING OF METHANE EXPLOSIONS

Laura Steeves
University of Kentucky, lj.steeves@outlook.com
Digital Object Identifier: https://doi.org/10.13023/etd.2019.139

STUDENT AGREEMENT:

I represent that my thesis or dissertation and abstract are my original work. Proper attribution has been given to all outside sources. I understand that I am solely responsible for obtaining any needed copyright permissions. I have obtained needed written permission statement(s) from the owner(s) of each third-party copyrighted matter to be included in my work, allowing electronic distribution (if such use is not permitted by the fair use doctrine) which will be submitted to UKnowledge as Additional File.

I hereby grant to The University of Kentucky and its agents the irrevocable, non-exclusive, and royalty-free license to archive and make accessible my work in whole or in part in all forms of media, now or hereafter known. I agree that the document mentioned above may be made available immediately for worldwide access unless an embargo applies.

I retain all other ownership rights to the copyright of my work. I also retain the right to use in future works (such as articles or books) all or part of my work. I understand that I am free to register the copyright to my work.

REVIEW, APPROVAL AND ACCEPTANCE

The document mentioned above has been reviewed and accepted by the student's advisor, on behalf of the advisory committee, and by the Director of Graduate Studies (DGS), on behalf of the program; we verify that this is the final, approved version of the student's thesis including all changes required by the advisory committee. The undersigned agree to abide by the statements above.

Laura Steeves, Student

Dr. Jhon Silva, Major Professor

Dr. Zacharias Agioutantis, Director of Graduate Studies

SIMPLIFYING TECHNIQUES APPLIED TO COMPUTATIONAL FLUID DYNAMICS MODELING OF METHANE EXPLOSIONS

THESIS

A thesis submitted in partial fulfillment of the
requirements for the degree of Master of Science in
Mining Engineering in the College of Engineering
at the University of Kentucky

By

Laura Steeves

Lexington, Kentucky

Director: Dr. Jhon Silva, Professor of Mining Engineering

Lexington, Kentucky

2019

ABSTRACT OF THESIS

SIMPLIFYING TECHNIQUES APPLIED TO COMPUTATIONAL FLUID DYNAMICS MODELING OF METHANE EXPLOSIONS

Traditional methods of studying underground coal mine explosions are limited to observations and data collected during experimental explosions. These experiments are expensive, time-consuming, and require major facilities, such as the Lake Lynn Experimental Mine. The development of computational fluid dynamics (CFD) modeling of explosions can help minimize the need for large-scale testing. This thesis utilized the commercial CFD software, SC/Tetra, to examine three case studies. The first case study modeled the combustion of methane in a scaled shock tube, measuring approximately 1 foot by 1 foot, by 20.5 feet long, with a methane cloud of 2.5 feet in length, at a concentration of 9% methane. The numerical results from the CFD model were in good agreement with experimental data gathered, with all pressure peaks within 0.25 psi of the recorded pressure data. However, the model had an extensive run-time of 16 hours to reach the peak pressures. The second case study modeled the same explosion, but utilized a total pressure boundary condition at the location of the membrane, instead of the combustion of methane. A pressure-time curve was assigned to this boundary, recreating the release of pressure by the explosion. This was made possible with the knowledge of the experimental data. The numerical results from the CFD model were in excellent agreement with experimental data gathered, with all pressure peaks within 0.07 psi of the recorded pressure data. Alternatively, this model had a run-time of 40 minutes. The third case study modeled a methane explosion in a large shock tube, measuring 8 feet by 8 feet, by 40 feet long, with a methane cloud of 4 feet in length, at a concentration of 9% methane. The bursting balloon technique was employed, which did not model the combustion of methane, but instead the equivalent energy release. The numerical results from the CFD model were in good agreement with the experimental data gathered, with all pressure peaks within 0.025 psi of the recorded pressure data. Additionally, the numerical results modeled the negative pressure phenomenon observed in the experimental results, caused by suction or negative pressure created by the blast wave, immediately following the positive wave. This model had a run-time of 20 minutes. The results of this researched provided validation that there are alternative ways to successfully model methane explosion, without having to model the chemical reactions involved in the combustion of methane, providing quicker run-times and in this case, more accurate results.

KEYWORDS: CFD Modeling, Methane Explosions, Explosion Pressures, Bursting Balloon Technique

Laura Steeves

04/26/2019

Date

SIMPLIFYING TECHNIQUES APPLIED TO COMPUTATIONAL FLUID DYNAMICS MODELING OF METHANE EXPLOSIONS

By
Laura Steeves

Dr. Jhon Silva
Director of Thesis

Dr. Zacharias Agioutantis
Director of Graduate Studies

04/26/2019
Date

DEDICATION

To my parents,
Celine and Paul,
For their endless support and encouragement.

ACKNOWLEDGMENTS

First, I would like to acknowledge the University of Kentucky Explosives Research Team. Without the dedication of each of its members, the safe and successful completion of my research would not have been possible. Second, I would like to acknowledge my advisor, Dr. Jhon Silva, who afforded me the opportunity to conduct this research, and who has challenged me and made each moment of graduate school unique and rewarding. I would also like to acknowledge Dr. Zacharias Agioutantis, and Dr. John Groppo for serving on my graduate committee. Finally, I would like to acknowledge the National Institute for Occupation Safety and Health, and the Alpha Foundation, for providing funding for projects which made this research possible.

TABLE OF CONTENTS

LIST OF TABLES

LIST OF FIGURES

CHAPTER 1. INTRODUCTION

Introduction

Computational Fluid Dynamics (CFD) modeling applications are presently used in the mining industry in areas such as mine ventilation, methane flow and control, dust dispersion and mineral processing (Xu, Luxbacher, Ragab, Xu, & Ding, 2016). Limited research has been conducted on CFD modeling applications for methane and coal dust explosions, which continue to be the most significant hazard in underground coal mines. Traditional methods of studying underground coal mine explosions are limited to observations and data collected during experimental explosions. These experiments are expensive, time consuming and require major facilities, such as the Lake Lynn Experimental Mine (LLEM), which is now closed. While there is still knowledge to gain regarding the nature and complexity of explosions in underground mines, CFD modeling can be used to minimize the need for large-scale testing, or to improve testing protocols.

The destructive overpressure caused by an explosion is not just the detonation pressure of a methane air mixture in the explosive range. The incident wave created by the initial explosion can have a much higher pressure load than the detonation pressure itself. Reflected waves from seals or the mine face and walls can cause increased pressure loads. The irregularity of mine tunnels, the roughness of the tunnel walls, and debris such as equipment, can create turbulence in the blast wave. The complexity of a mine environment with crosscuts, entries, and angles can cause multiple wave fronts to form after an explosion, producing a much more complex pressure-time history than idealized (McMahon, Britt, & Walker, 2010). The successful simulation of these catastrophic events would help the mining industry better understand the behavior of explosions, explore ways

to prevent or control them in the worst case scenarios, and ultimately help prevent the loss of life.

This thesis focuses on the exploration of the application of CFD modeling to underground methane explosions using the commercial CFD software SC/Tetra, and presents three case studies. All models were calibrated with experimental data gathered for this thesis. The first case study models the combustion of methane in a scaled shock tube. The second case study models the same methane explosion, using a total pressure boundary condition at the location of the membrane, instead of the physical combustion of methane. Finally, the third case study models a larger scale methane explosion, using the bursting balloon technique, which does not model the combustion of methane, but instead the equivalent energy release. This work demonstrates the validation of using CFD to model methane explosions, and presents ways to simplify the model to optimize the computational run-time, while achieving equivalent results.

The Hazard of Explosions in Underground Coal Mines

The United States mining industry practices have emphasized the prevention of explosions in underground coal mines, instead of mitigation. The prevention practices include mine ventilation regulations and frequent inspections of underground coal mines. Despite successful practices for the prevention of underground coal mine explosions in the US, the threat of an explosion does still exist.

1.1.1 Methane Explosions

Coal deposits release significant amounts of methane gas, which has an explosive range of 5%-15% when mixed with air containing at least 12.1% oxygen (Brune,

Cashdollar, & Zipf, 2007). In order for a methane explosion to occur, there must be a methane accumulation within the explosive range, there must be sufficient oxygen in the air, and there must be an ignition source. Although there are measures in place to prevent the accumulation of methane, these systems can fail. When ventilation systems fail and are not corrected immediately, methane can accumulate to explosive levels. Methane can also accumulate in the gob area, or in random pockets. These accumulations of methane in the explosive range can be ignited by various sources, such as an electric spark, or a machine tooth scrapping hard rock (Kissell, Tien, & Thimons, 2007). Methane and air mixtures can produce violent explosions even without transitioning into a coal dust explosion.

1.1.2 Coal Dust Explosions

A coal dust explosion has been defined as the uncontrolled exothermic combustion in air of ultra-fine particles of coal in which the resultant aerodynamic disturbance disperses additional coal dust into the air, thus fueling the combustion in a self-sustaining process (Kruger, Plessis, & Vassard, 1996). For a coal dust explosion to occur, the concentration of coal dust in a cloud must be enough to propagate the flame, there must be sufficient oxygen in the air, there must be an ignition source, such as a flame, hot surface, or electric spark, and the dust must have a low moisture content. Coal dust explosions are often more disastrous than methane explosions because of their longer duration and high temperature. The turbulence caused by a localized gas (methane) or coal dust explosion kicks dust up into the air, from the floor or ribs, creating dust clouds. These clouds are then in the direct path of the flame, acting as fuel for the explosion, and causing extensive explosions from propagation (Hartmann, 1954).

Overview of Recent Mine Explosions in the USA

In the last two decades, three major mine explosion disasters have occurred in the USA; The Sago Mine disaster (2006), the Darby Mine disaster (2006), and the Upper Big Branch Mine disaster (2010). A brief overview of these disasters is given below.

1.1.3 The Sago Mine Disaster

On January 2nd, 2006, a thunderstorm travelled through Upshur County, West Virginia, where the International Coal Group's Sago Coal Mine was located. At approximately 6:26 a.m., lightning strikes were recorded within five miles of the mine portal. At one instant, an exceptionally powerful lightning strike hit, and a cloud of methane was ignited in a recently sealed area of the Sago mine (McActeer, 2006). Investigators later came to the conclusion that the energy from the lightning strike was most likely transferred onto an abandoned pump cable in the sealed area, which ignited an explosive concentration of methane behind the seals. The methane explosion was so powerful that it completely destroyed all ten erected seals (MSHA, 2007).

Twenty-nine miners were underground at the time of the explosion. One miner was immediately killed due to the blast. Sixteen other miners who were not significantly injured by the blast, and who were further away from the ignition source, were able to walk out of the mine to safety. The twelve other miners underground attempted to exit the mine, but were forced to barricade themselves to prevent poisonous gases from reaching them. Before rescuers could reach them, eleven of the miners succumbed to carbon monoxide asphyxiation (McActeer, 2006).

1.1.4 The Darby Mine Disaster

An explosion occurred in the sealed A Left Section of the Darby Mine No. 1 in Harlan County, Kentucky, on May 20th, 2006. Six miners were underground at the time of the explosion. Five miners received fatal injuries as a result of the explosion, and one survived (Light, Herndon, & Guley, 2007).

Evidence found indicated that two men had been using oxygen-acetylene torches to remove metal roof straps that intersected the No. 1 and No. 3 seals. The cutting torch would have provided an ignition source for an explosive concentration of methane. Since there was no way to test the air behind the No. 3 seal, the cutting torch should not have been used in close proximity to the seal. The other four men underground at the time heard the explosion and began to exit the mine. However, when their carrier became lodged in debris, they began to travel on foot. One of the men was located by rescuers and was taken out of the mine. The other three men eventually succumbed to carbon monoxide poisoning at different locations in the mine (Light, Herndon, & Guley, 2007).

1.1.5 The Upper Big Branch Mine Disaster

The Upper Big Branch Mine, located in West Virginia, was the site of the worst mining disaster in the last forty years in the United States. The disaster occurred on April 5th, 2010, at approximately 3:02 p.m. and killed twenty-nine miners (O'Brien, 2011).

The explosion originated when a concentration of methane gas within the explosive range was ignited, likely by a spark produced from the longwall shearer cutting sandstone from the roof, or from rock on rock contact during a sandstone roof fall in the gob area. The concentration of methane gas was suspected to have been liberated from the floor behind the longwall shields. The gas then flowed to the return behind the shields, where it

became restricted by a roof fall. This likely caused gas to accumulate close to where the shearer was operating. The accumulation of methane was not detected by any methane monitors on the machine (WVMHS&T, 2011).

The explosion most likely began in the gob area behind the longwall shields, and then propagated in all directions. It then transitioned into a coal dust explosion which is believed to have been the principle source of fuel for propagating the explosion. The fine coal dust likely came from rib spalling (WVMHS&T, 2011). All twenty-nine miners were killed as a result of this explosion.

Research Significance

There is still uncertainty concerning the amount of pressure that is expected to be generated by an explosion, and the actual pressures experienced during the disasters discussed previously. This information is crucial because it concerns the design of equipment used underground, such as communication and tracking devices, or structures built underground, such as seals, and refuge chambers. Being able to accurately model explosions can be used to identify the pressures devices or structures need to withstand for worst case scenarios. This is critical to ensuring the safety of miners underground.

Additionally, this research presents a way to model methane explosions without having to model the chemical reactions involved, which require a smaller mesh, more computational power, and longer run times. This will allow for more extensive modeling of entire mine networks, and easier model calibration.

Research Limitations

The CFD model of the first case study assumed that the methane-air mixture within the methane-air zone was uniform and that the reading from the MX6 iBRID gas detector was representative of the concentration of methane. This reading was used as the percent methane value assigned to the methane-air volume in the model. It was not possible to determine if there were any pockets of higher or lower concentrations of gas in the methane-air mixture, which could have had an effect on the pressure profile produced by the mixture. Methane explosions are extremely volatile, mainly because of the unpredictability of the pockets of methane in the explosive range, however, this assumption was necessary for practical modeling at this time.

Additionally, validation of this research was limited to the University of Kentucky Explosive Research Team (UKERT) test facilities, including the scaled shock tube, and the large shock tube. Neither of these testing environments allowed for the continued propagation of a methane explosion, where the explosion could transition from deflagration to detonation. Similarly, validation of this research in proper mine geometry was also limited.

Research Procedures

Three case studies were investigated in this thesis which utilized the commercial CFD modeling software, SC/Tetra. The first case study modeled the combustion of methane in a scaled shock tube. Experimental data was gathered using piezoelectric sensors to record the pressure vs. time history of a methane explosion, which had a two-and-a-half-foot-long cloud, and a methane concentration of 9%. The model was calibrated to the data collected at three pressure sensor locations. The second case study modeled the same

methane explosion, using a total pressure boundary condition at the location of the membrane, instead of the physical combustion of methane. This technique allowed for a total pressure vs. time curve to be assigned to this boundary, simulating the release of pressure from the explosion. This model was also calibrated to the data collected at three pressure sensor locations. The third case study modeled a methane explosion in a large shock tube. Experimental data was gathered using piezoelectric sensors to record the pressure vs. time history of the explosion, which had a 4-foot-long cloud, and a methane concentration of 9%. The bursting balloon CFD technique was used, which does not model the combustion of methane, but instead the equivalent release of energy from a specific volume. The model was calibrated to the data collected at two pressure sensor locations.

CHAPTER 2. LITERATURE REVIEW

Chapter 2 provides a comprehensive review of previous work done using CFD to model explosions, and provides valuable information regarding modeling considerations. This includes methane explosions, where the combustion of methane is modeled, and high explosives explosions, where the bursting balloon technique is employed.

CFD Governing Equations

CFD modeling of explosions uses four governing equations, which are based on the conservation laws of physics. The governing equations are conservation of mass, momentum, energy, and species, seen below (Diaz-Ovalle, Lopez-Molina, & Vazquez-Roman, 2016).

Continuity:
$$\frac{\partial \rho}{\partial t} = \nabla \cdot \rho \mathrm{v} \tag{1}$$

Momentum Conservation
$$\frac{\partial}{\partial t}(\rho \mathrm{v}) = -\nabla \cdot \rho \mathrm{vv} - \nabla P - \nabla \cdot \tau - \rho \mathrm{g} \tag{2}$$

Energy Conservation
$$\frac{\partial}{\partial t}(\rho C_P T) = -\nabla \cdot (\rho C_P T \mathrm{v}) - \nabla \cdot \mathrm{q} - \tau : \nabla \mathrm{v} \tag{3}$$

Species i Conservation
$$\frac{\partial}{\partial t}(\rho Y_i) + \nabla \cdot (\rho Y_i \mathrm{v}) = -\nabla \cdot \mathrm{J_i} \tag{4}$$

Where t is time, v is velocity vector, P is pressure, τ is shear stress tensor, g is gravitational acceleration vector, T is temperature, q is heat flux vector, Y is mass fraction per species i, ρ is density, and C_P is specific heat capacity.

The nonlinearities in the momentum equation are due to the turbulence, which is caused by walls and obstacles adjacent to the fluid. The k-ε turbulence model contains two

equations, which includes a variation in the turbulent kinetic energy, k, and can be seen below (Laundry & Sharma, 1974).

$$\frac{\partial k}{\partial t} + \mathrm{v} \cdot \nabla k = \tau : \nabla \mathrm{v} - \varepsilon + \nabla \cdot ((v + v_T)\nabla k) \tag{5}$$

$$\frac{\partial \varepsilon}{\partial t} + \mathrm{v} \cdot \nabla \varepsilon = 1.44\left(\frac{\varepsilon}{k}\right)\tau : \nabla \mathrm{v} - 1.92\left(\frac{\varepsilon^2}{k}\right) + \nabla \cdot \left(\left(v + \frac{v_T}{1.3}\right)\nabla \varepsilon\right) \tag{6}$$

Where v is kinematic viscosity and v_T is turbulent kinematic viscosity that is calculated by the following equation:

$$v_T = 0.09\left(\frac{k^2}{\varepsilon}\right) \tag{7}$$

Methane Explosion Modeling Considerations

2.1.1 Methane Explosion Chemistry

The chemical reaction for an ideal stoichiometric mixture of approximately 10% by volume of methane in air is given by (Zipf, Sapko, & Brune, 2007):

$$CH_4 + 2O_2 \rightarrow CO_2 + 2H_2O + Energy$$

For reference, the energy content of a one cubic meter of an ideal methane-air mixture is about the same as 0.75 kg of TNT (Zipf, Sapko, & Brune, 2007).

2.1.2 Methane Concentration

Experimental methane explosion data was collected by NIOSH using a 120-liter test chamber. The absolute explosion pressure was recorded for the combustion of nonstoichiometric, and stoichiometric methane-air mixtures. Nonstoichiometric methane-air mixtures produced lower temperature and pressure increases. From Figure 2-1, the maximum absolute explosion pressure occurred at approximately 10% methane, which is

slightly above stoichiometric proportions of 9.5%. Gas liberated in coal mines typically consists of 90% methane, and can also contain alkanes such as ethane, propane, butane, and pentane. These hydrocarbons can increase the energy released, and result in a higher pressure. On the contrary, the gas liberated may also contain carbon dioxide, which can lessen the increase in pressure. These effects were considered to be negligible (Cashdollar, Zlochower, Green, Thomas, & Hertzberg, 2000).

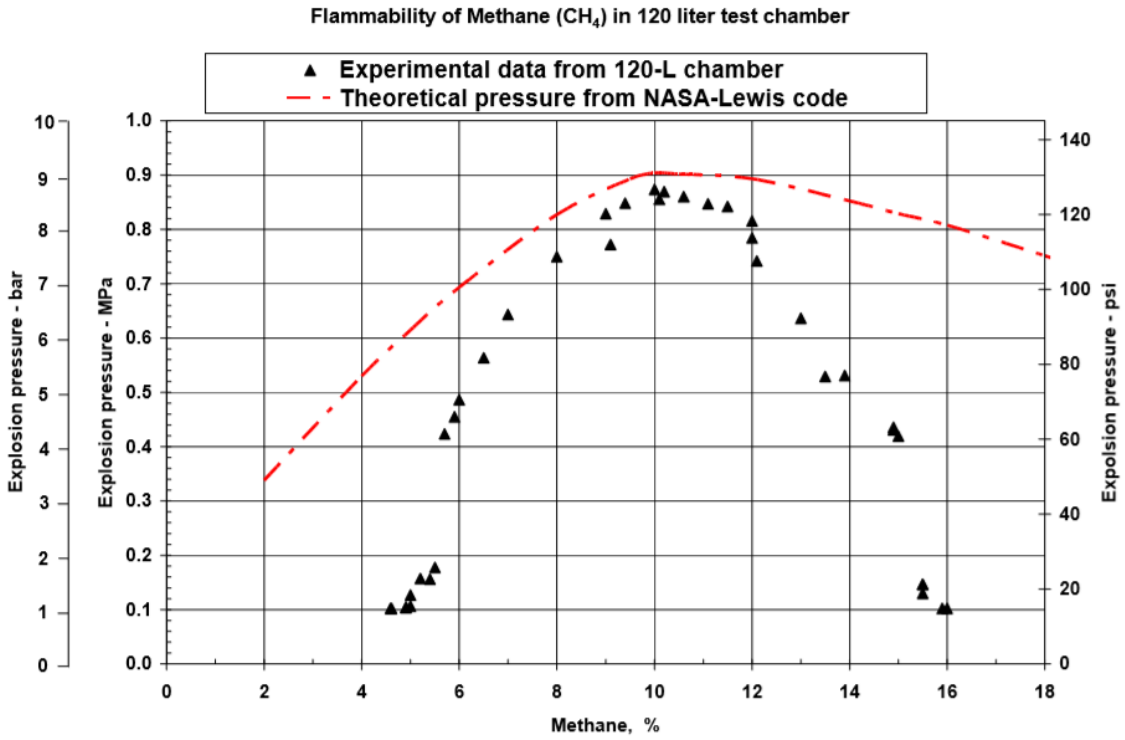

Figure 2-1: Variation of Absolute Pressure vs. Methane Concentration: Theoretical and Experimental Determinations (Cashdollar, Zlochower, Green, Thomas, & Hertzberg, 2000)

From Figure 2-1, the experimental data gathered was slightly less than the theoretical calculations. This could be attributed to incomplete combustion and heat loss during the experiments. As it is not possible to know the exact composition of a methane-air mixture in a mine environment, it is necessary to plan for the highest potential explosion pressure, i.e., the pressure developed by the ideal stoichiometric mixture. For this reason,

during any experimental or theoretical testing, a methane concentration of 9.5% was desired.

2.1.3 Turbulence and Pressure Piling

Experimental data collected in a closed spherical vessel, such as the 120-liter chamber discussed previously, is not assumed to be the maximum pressure that can be achieved by methane and methane coal dust explosions. Since these vessels are spherical, it is assumed that the dynamic effects due to pressure waves are negligible. Also, it is assumed that the ignition occurs at the center of the vessel, and the flame speed is well below the speed of sound (Zipf, Sapko, & Brune, 2007). In a mine environment, the ignition of a methane-air mixture propagates through mine entries/tunnels, which is much more complex than an explosion in a controlled vessel. Two factors that contribute to the complexity of an explosion underground are turbulence and pressure piling. The turbulence is dependent on the flow velocity and the roughness of the tunnel walls. Increased turbulence will increase the combustion rate, in turn increasing the speed of the flame front. Pressure piling occurs when the flame front is travelling towards a dead end such as a seal or a mine face. The combustion front acts as a piston, compressing the unburned gas in front of it, causing the static pressure inside this region to increase (Zipf, Sapko, & Brune, 2007). From the information gathered, it was apparent that turbulence must be considered in the model, and the simulated fluid must be compressible. Figure 2-2 below displays the positive feedback loop discussed between pressure increase, turbulence, and combustion rate.

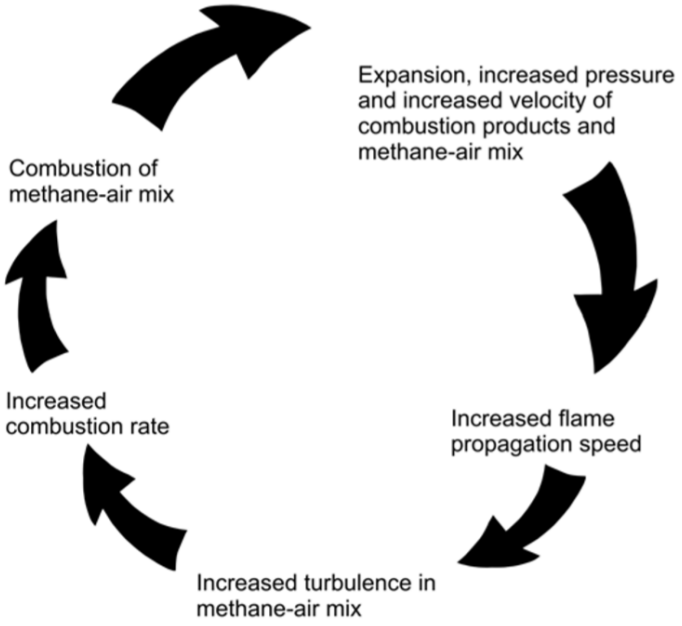

Figure 2-2: Positive Feedback Loop Between Pressure Increase, Turbulence, and Combustion Rate (Zipf, Sapko, & Brune, 2007)

In addition to turbulence and pressure piling, the volume of the explosive methane-air mixture, and the degree of confinement also affect the level of explosion pressure. Larger volumes of explosive gas will provide higher pressures (Zipf, Sapko, & Brune, 2007). As mentioned previously, the energy content of one cubic meter of an ideal methane-air mixture is equivalent to 0.75 kg of TNT (Zipf, Sapko, & Brune, 2007). If an explosion occurs in open air, the reaction gases can expand freely, but if the explosion occurs in a confined space or partially confined space, the expanding reaction gases cause an increase in pressure (Zipf, Sapko, & Brune, 2007).

NIOSH Methane Explosion Modeling Platforms: AutoReaGas and FLACS

The National Institute for Occupational Safety and Health (NIOSH) researchers have used two gas explosion modeling platforms to extrapolate small-volume gas explosion data to larger gas explosions. These modeling platforms are AutoReaGas, from Century

Dynamics, Inc. (2007), and FLACS (Flame Acceleration Simulator), from GexCon (2007a). Typically used in the oil, gas, and chemical industries, AutoReaGas and FLACS both are CFD models that numerically solve partial differential equations governing gas explosions. This allows for risk assessment and mitigation measures for different gas explosion scenarios. There is limited work utilizing these models for a mining industry application.

AutoReaGas and FLACS consist of three elements: (1) The Reynolds-averaged Navier-Stokes equations, which describe fluid flow and the conservation of mass, momentum, and energy for a differential volume in terms of pressure, temperature, gas density, and velocity. (2) A turbulence model, which describes the dissipation rate of turbulence kinetic energy (both models utilize the k-ε turbulence model). (3) An empirical turbulent flamelet model, which is a combustion model that describes the concentration change rates of the reactant and product species, and the related energy release rate (Zipf, Sapko, & Brune, 2007). AutoReaGas uses an empirical relationship between reaction rate and flame speed, while FLACS uses a "β flame model" which correlates turbulence burning velocity with turbulence parameters. In both cases, an increase in turbulence kinetic energy causes an increase in the reaction rate. One downfall of these models is their inability to properly consider the physics of detonation or detonation to deflagration (Zipf, Sapko, & Brune, 2007).

NIOSH Methane Explosion Modeling Calibration

Six methane gas explosion tests were conducted in the LLEM. AutoReaGas and FLACS models were used to attempt to duplicate the recorded pressure vs. time histories at different points. Each of the six tests involved a larger volume of the explosive methane-

air mixture, ranging from 3.7 to 18.3 meters (12 to 60 feet), and had a concentration of methane of approximately 10%. Additionally, some tests utilized only one drift, while others used three.

The numerical results from AutoReaGas agreed with the experimental results to within ±47%, while the numerical results from FLACS agreed with the experimental results to within ±24% (Zipf, Sapko, & Brune, 2007). The modeling done in FLACS was completed "blind", meaning there was no foreknowledge of the experimental measured pressures.

Figure 2-3, Figure 2-4, and Figure 2-5 below show the experimental results from LLEM for three tests of different magnitudes, the numerical results from AutoReaGas, and the numerical results from FLACS respectively.

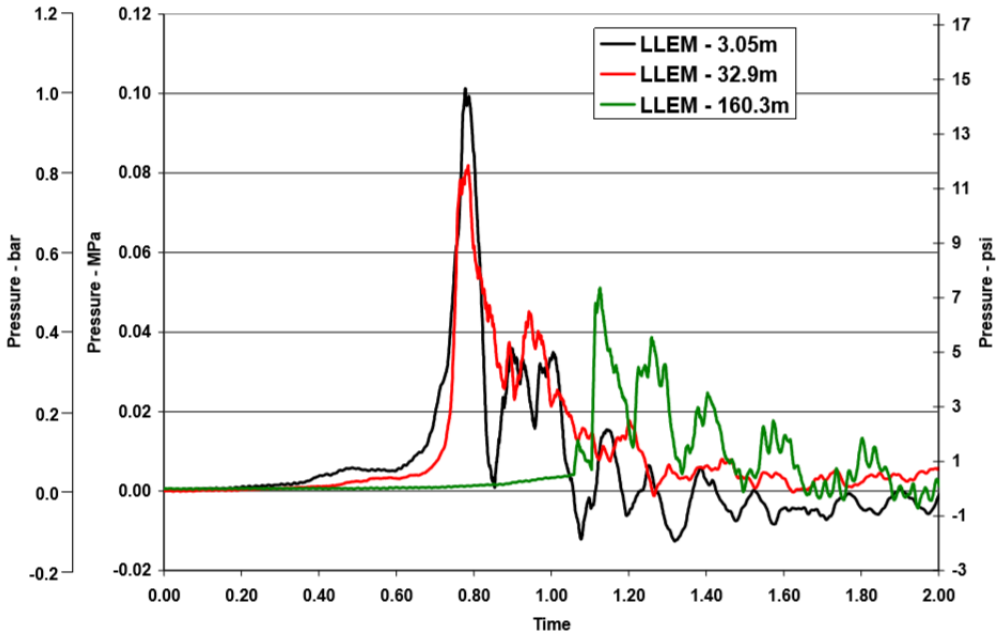

Figure 2-3: Lake Lynn Experimental Mine Calibration Data (Zipf, Sapko, & Brune, 2007)

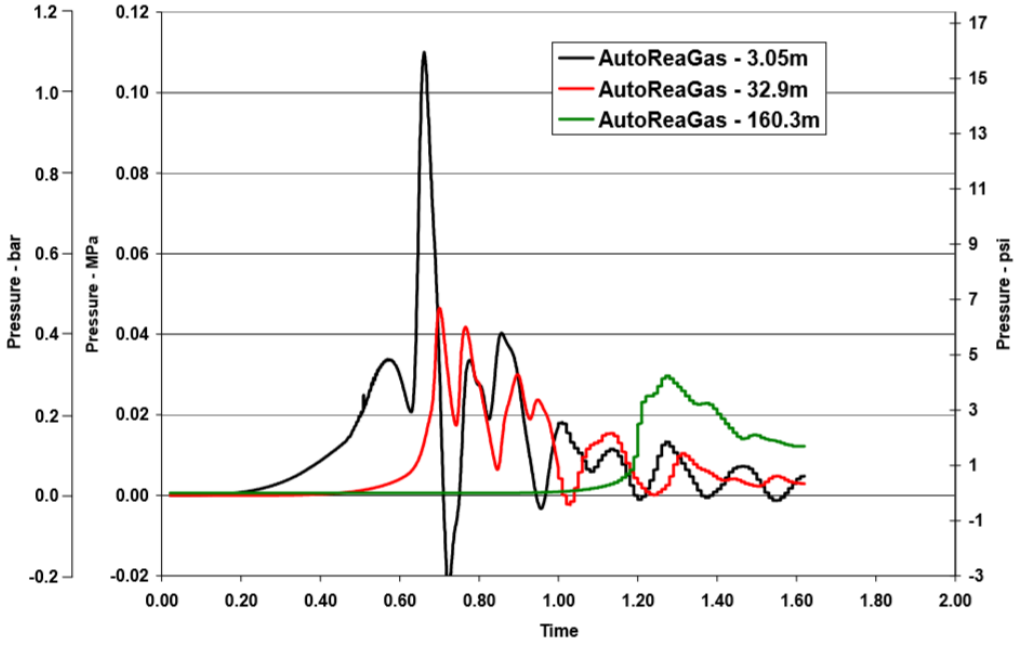

Figure 2-4: Calculations from AutoReaGas Model (Zipf, Sapko, & Brune, 2007)

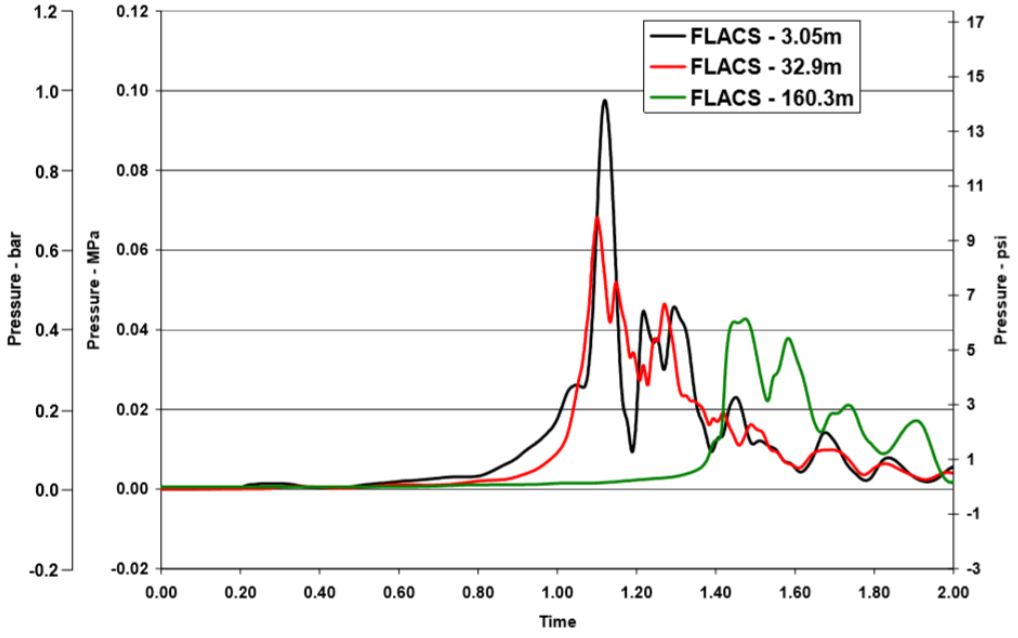

Figure 2-5: Calculations from FLACS Model (Zipf, Sapko, & Brune, 2007)

The experimental and model data compared well in terms of peak pressures achieved, as well as the duration and shape of the pressure waves. However, the arrival time of the pressure waves was inaccurate. This could be attributed to the nature of the ignition of the explosion. The model used a single-point ignition source, whereas the test used an electric match, which would have dispersed several sparks to initiate the explosion in many locations. Overall, these gas explosion models were considered to have reproduced the measured experimental data well (Zipf, Sapko, & Brune, 2007).

NIOSH Methane Explosion Modeling of Large Gas Cloud Volumes

From the successful calibration of these models, larger volumes of confined explosive mixtures were examined using AutoReaGas and FLACS. Seals were erected in the model to create confinement. The methane clouds modeled were 41, 71, 161, 228, and 300 meters in length. The pressure-time histories at the seal locations were recorded by the model. The highest pressure calculated was 653 psi, from a reflected detonation wave. At a pressure that high, it was very likely that the explosion would have transitioned from deflagration to detonation. Figure 2-6 and Figure 2-7 below show the simulated results at one of the seals for various cloud sizes, in AutoReaGas and FLACS respectively.

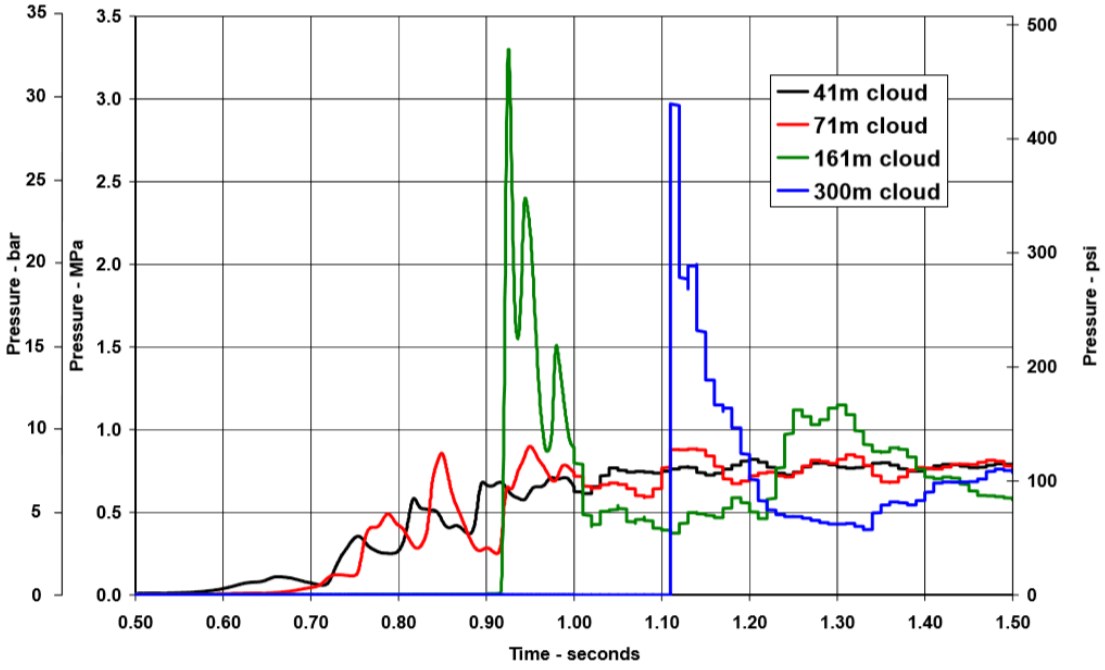

Figure 2-6: Pressure vs. Time History at Seal B – Various Cloud Sizes (AutoReaGas) (Zipf, Sapko, & Brune, 2007)

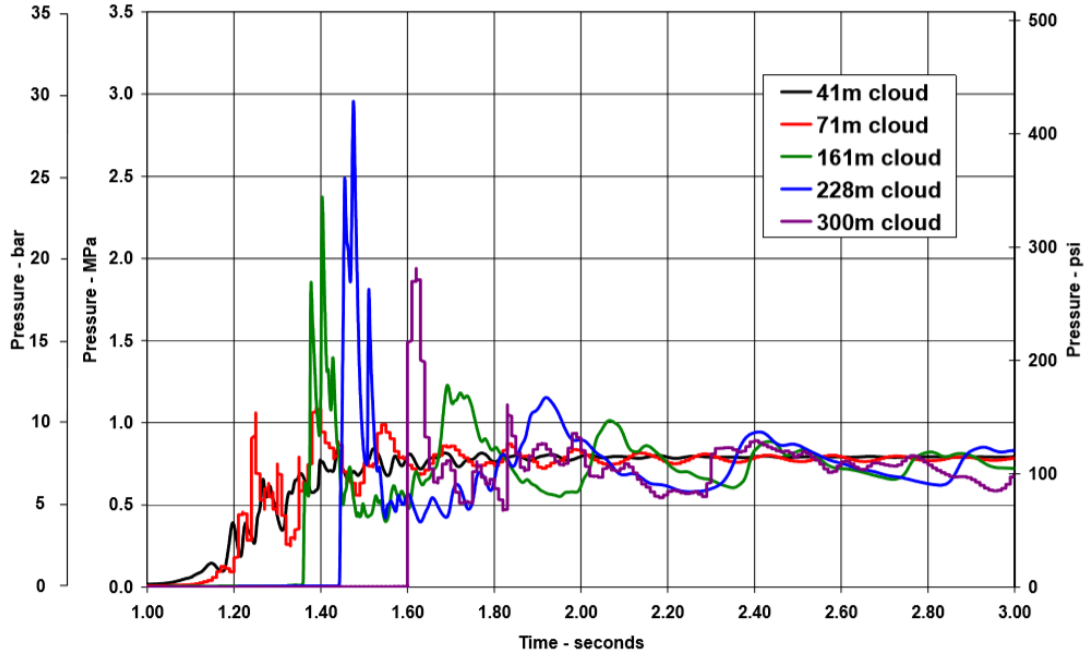

Figure 2-7: Pressure vs. Time History at Seal B – Various Cloud Sizes (FLACS) (Zipf, Sapko, & Brune, 2007)

Upper Big Branch Mine Explosion Case Study Using FLACS

After the 2010 Upper Big Branch mine explosion, FLACS CFD solver was used to conduct a detailed explosion analysis to evaluate the overpressure development through the mine. FLACS used the compressible Reynolds-Averaged Navier-Stokes (RANS) equations (conservation of mass, momentum, energy, and species) on a 3D Cartesian grid using the finite volume method. The RANS equations were closed using the k-ε turbulence model, and the SIMPLE pressure correction method was applied. Additionally, FLACS contained a flamelet-based combustion model with one-step reaction kinetics (Davis, Engel, & Wingerden, 2015). As mentioned previously, FLACS had been validated against mine explosion experiments in the LLEM.

This study demonstrated that regions within crosscuts between entries experienced very high pressures due to the flame front arrival from both directions, creating a significant pressurization. This caused significant flow and drag forces in the direction of the advancing blast wave, and against it. This flow reversal accounted for the blast indicators from the aftermath of the explosion that contradicted the intuitive flow of the explosion through the mine. These results confirmed that as the complexity of the mine geometry increases, the explosion dynamics become increasingly difficult to interpret intuitively (Davis, Engel, & Wingerden, 2015).

Figure 2-8 below displays the results obtained by FLACS compared with the experimental results from the LLEM for tests 470 and 485. The results were in very good agreement.

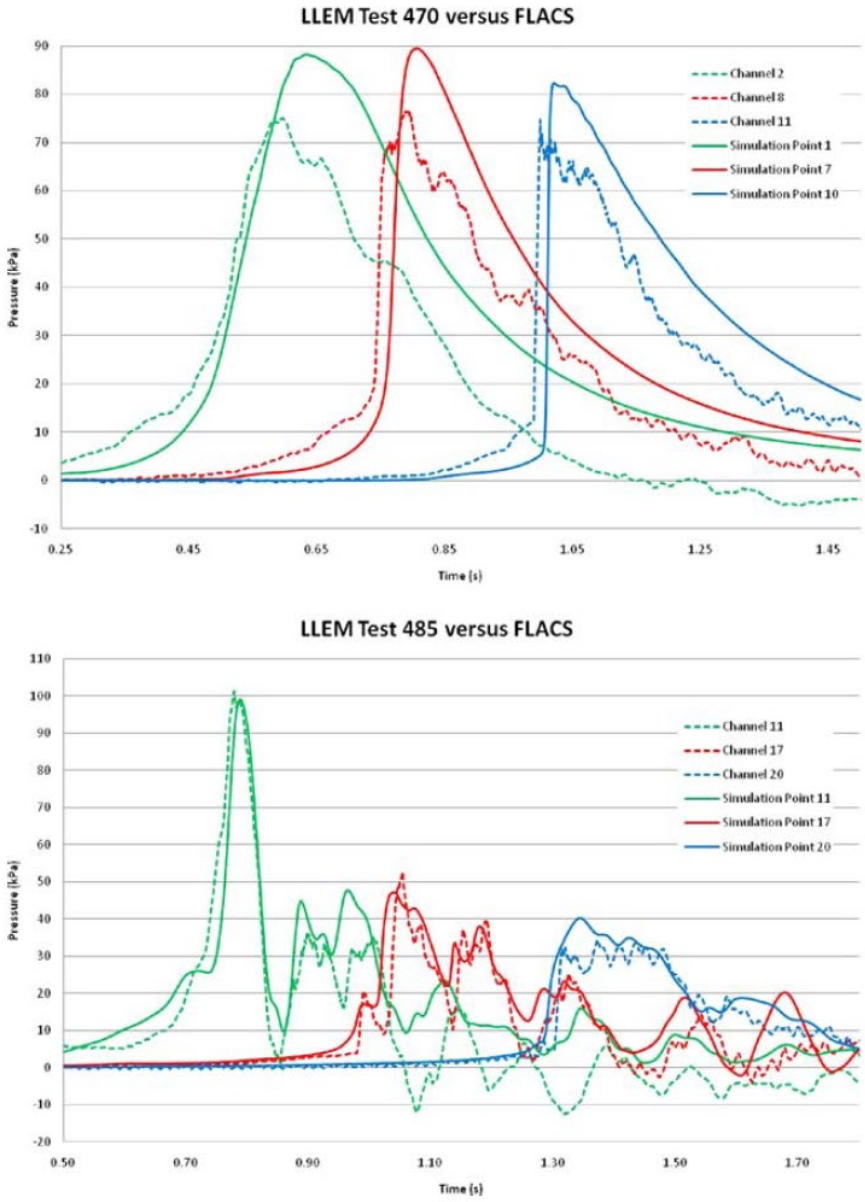

Figure 2-8: LLEM Experimental Data vs. FLACS Simulation Data (Davis, Engel, & Wingerden, 2015)

Methane Explosion Simulation in Complex Geometry Using ANSYS FLUENT

A study focused on using CFD to model the propagation of a methane-air mixture combustion wave in a complex geometry was completed using ANSYS FLUENT. A methane explosion in a family house was modeled, and was compared with experimental

data gathered by pressure sensors. The three-dimensional problem was solved by the finite element method (Kozubkova, Krutil, & Nevrly, 2014).

The results of the simulation were in very good agreement with the experimental results in terms of time and overpressure absolute values. From the experiment, the peak pressure recorded was 1800 Pa, at 35.05 s, and from the numerical model, this value was 1834 Pa at 34.95 s. Additionally, the rapid decrease in overpressure observed at the end of the pressure wave due to the damage imposed on the house was very well captured (Kozubkova, Krutil, & Nevrly, 2014).

Bursting Balloon Technique Applied to Counter Terrorism

The bursting balloon CFD technique has been applied to model terrorist bombing attacks in order to assess the structural response of transportation networks, and the risk of human injury. The finite element code Europlexus was employed. The bursting balloon technique utilized a compressed balloon, which was then released, producing a pressure-time function that matched the air blast history. The amount of initial compression, or pressure applied to this balloon was calibrated with the impulse. This method provided an alternative CFD method with a shorter computational run-time, in comparison with other models (Solomos, Casadei, Giannopoulos, & Larcher, 2011). This method was preferred because larger dimension finite elements could be used, lessening the computational run-time, while still modeling the structure and fluid.

CHAPTER 3. EXPERIMENTAL SETUP

Chapter 3 outlines the experimental setup for testing completed in two UKERT explosion testing facilities. The first is the scaled shock tube, and the second is the large shock tube. Methane explosion testing was conducted in both facilities.

Scaled Shock Tube Setup

While the large shock tube was being constructed, UKERT conducted methane explosion testing in a scaled shock tube, measuring 10.875 inches by 11 inches, and 19 feet long. This shock tube was used to collect experimental data for this research. A 1-foot-long closed-end section was constructed and added to the end of the shock tube which housed the manual mixing fan, and the methane gas inlet. Additionally, a 6-inch-long addition was constructed to create a longer methane-air mixture zone. Fully assembled, the shock tube was 20.5 feet long. The opposite end of the scaled shock tube was open.

3.1.1 Methane Concentration

As mentioned previously, it is necessary to plan for the highest potential explosion pressure, which occurs when the methane-air mixture is an ideal stoichiometric mixture. Therefore, the objective methane concentration for testing was 9.5% methane by volume. The methane entered the bottom of the scaled shock tube through a gas line, where a ball valve was used to control the inflow of methane. To achieve a homogeneous mixture, a mixing fan was manufactured and installed in the end of the scaled shock tube where the methane entered the methane-air zone.

3.1.1.1 Mixing Fan

A fan blade was constructed of steel and positioned inside the closed end of the scale shock tube where the methane-air mixture occurred. The fan was controlled by an axis extending out of the closed end. An impact drill was used to spin the axis as methane was added to help produce a uniform mixture. Figure 3-1 below shows the blade of the mixing fan on the end of the shock tube.

Figure 3-1: Scaled Shock Tube Mixing Fan Blade

3.1.2 Membrane Material

The membrane was used to separate the methane-air mixture from the outside atmosphere and allowed the mixture to reach the explosive limit of methane (5%-15%). The membrane had to be thin enough to rupture upon ignition of the methane, so that the explosion could reach the open end of the shock tube. A hard plastic material was tested, but it was determined that the material did not rupture easily enough for the desired purposes. Then, a typical black trash bag material with a thickness of 2 mil was used, and

had good results. The membrane was positioned in the scaled shock tube two and a half feet from the closed-end, creating a methane-air mixture volume of approximately 2.5 ft^3 or 0.7 m^3. The membrane can be seen in Figure 3-2 below, before and after ignition of the methane-air mixture.

Figure 3-2: Black Trash Bag Membrane Before and After Ignition

3.1.3 Gas Detectors

UKERT utilized industrial scientific MX6 iBRID gas detectors with infrared methane sensors to monitor the methane concentration in the methane-air mixture zone. These devices were capable of reading percent methane by volume from zero to one hundred percent. Each device was equipped with a pump, which allowed readings to be taken with tubing at monitoring points along the length of the shock tube (within the methane-air mixture zone). UKERT had four of these devices available, however, typical testing in the scale shock tube only required the use of two methane detectors to determine the concentration in the methane-air mixture zone. Based on the ideal stoichiometric mixture of methane in air, the desired methane concentration before ignition was 9.5% methane by volume. The pump tubing was removed from the shock tube prior to ignition

to protect the devices. Figure 3-3 below shows two MX6 iBRID methane gas detectors on the ground, with their pump tubing leading to the monitoring points within the methane-air mixture zone.

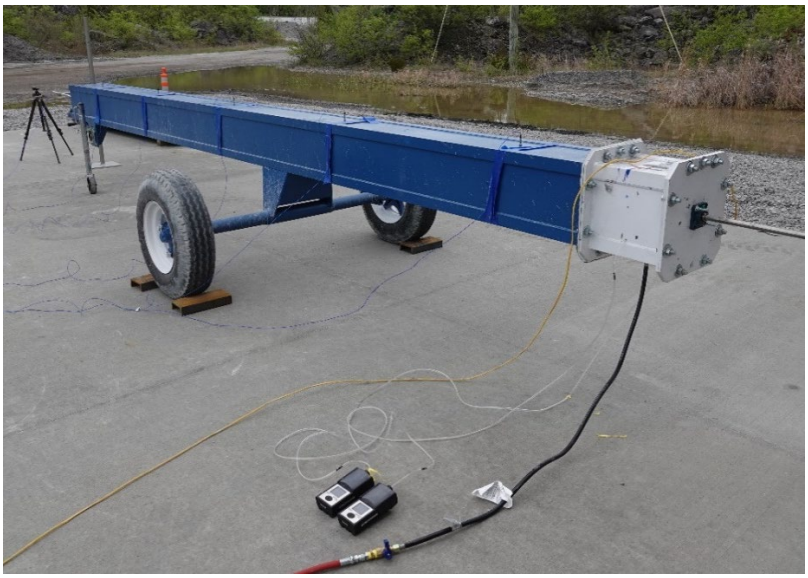

Figure 3-3: MX6 iBRID Methane Gas Detectors Setup

3.1.4 Igniters

As mentioned previously, in order for a methane and coal dust explosion to occur, an ignition source is needed. Two types of igniters were investigated, a 5 KJ igniter, and an electric match. The 5 KJ igniter used a small amount of explosives to ignite the mixture. The electric match used an externally applied electric current to ignite a combustible compound, providing a source of heat. It was determined that the 5 KJ igniter, in this case, may release too much energy, causing the membrane to rupture, instead of the methane explosion itself. The electric match did not provide too much added energy to the explosion, and properly ignited the methane-air mixture, allowing its own force to rupture the membrane. Therefore, the electric match was used at the igniter for testing in the scaled

shock tube. One electric match was placed approximately 6 inches from the top of the shock tube within the methane-air mixture zone.

3.1.5 Pressure Sensors

The shock tube was equipped with five locations for PCB Piezotronic dynamic pressure sensors to be installed in the roof. Each location was spaced 4 feet apart, with the last location being 1.5 feet from the open end of the shock tube. The pressure sensors were threaded into place until the diaphragm of the sensor was flush with the interior wall to prevent reflective pressure waves from occurring. For experimentation in the scaled shock tube, pressure sensors with peak measuring pressures of 50 psi were used, as pressures higher than 50 psi were not expected. For this experiment, five pressure sensors were installed, and each had a designated signal channel, with channel 1 being closest to the membrane, and channel 5 being farthest. The experimental setup can be seen in Figure 3-4 below, with the locations of the igniter, membrane, and pressure sensors, and their designated channels.

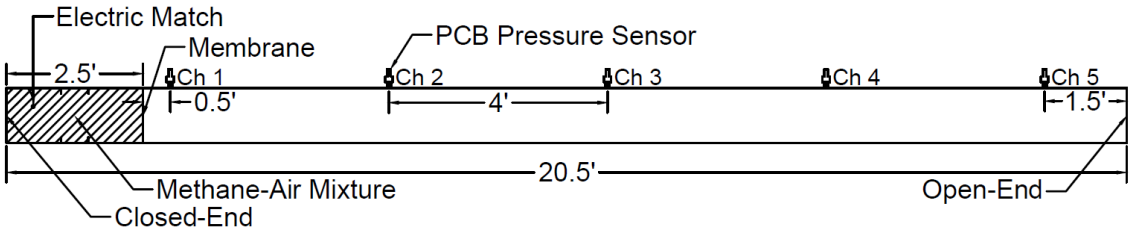

Figure 3-4: Scaled Shock Tube Experimental Setup

3.1.6 Data Acquisition Instrumentation

In order to gather the data from the pressure sensors, a data acquisition system was used. The pressure sensors were connected to a signal conditioner which provided power to the sensors and transferred the recorded signals to the DataTrap. The DataTrap was

programmed to record these signals when an increase or decrease in pressure occurred. These recordings were then downloaded from the DataTrap onto a laptop, where they were analyzed using Dplot. Figure 3-5: Data Acquisition System (Yonts, 2018) below displays a general representation of the data acquisition system used.

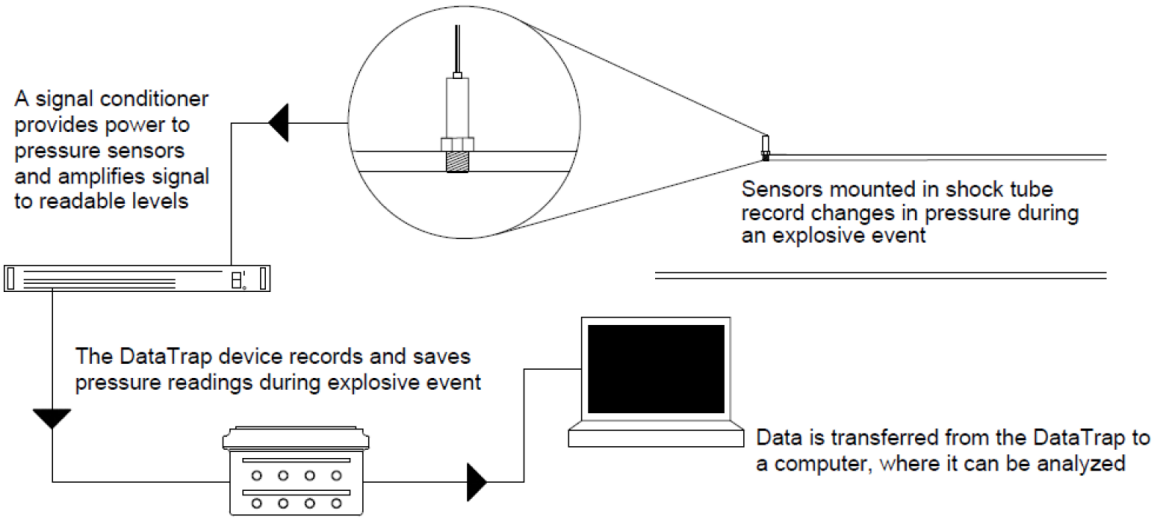

Figure 3-5: Data Acquisition System (Yonts, 2018)

The experimental results gathered from the methane explosion test in the scaled shock tube can be found in Chapter 4.

Large Shock Tube Setup

The large shock tube was constructed by UKERT in order to conduct full-scale methane and coal dust explosion testing. With the closing of the NIOSH Lake Lynn Experimental Mine, these facilities are increasingly valuable. The option of constructing a tunnel in an underground limestone mine was considered, however, given safety considerations for explosions using mixtures of gases, it was decided to construct the shock tube on the surface of the limestone mine in Georgetown, Kentucky.

3.1.7 Large Shock Tube Dimensions

The interior dimensions of the large shock tube measure 8 feet by 8 feet, and 40 feet long. The shock tube was built in two twenty foot sections so that it could be moved if necessary. The interior walls are made up of one-quarter inch thick steel, and the shock tube is designed to withstand up to 250 psi. One end of the shock tube is closed, and the other is open. Figure 3-6 below displays the design of one of the shock tube sections.

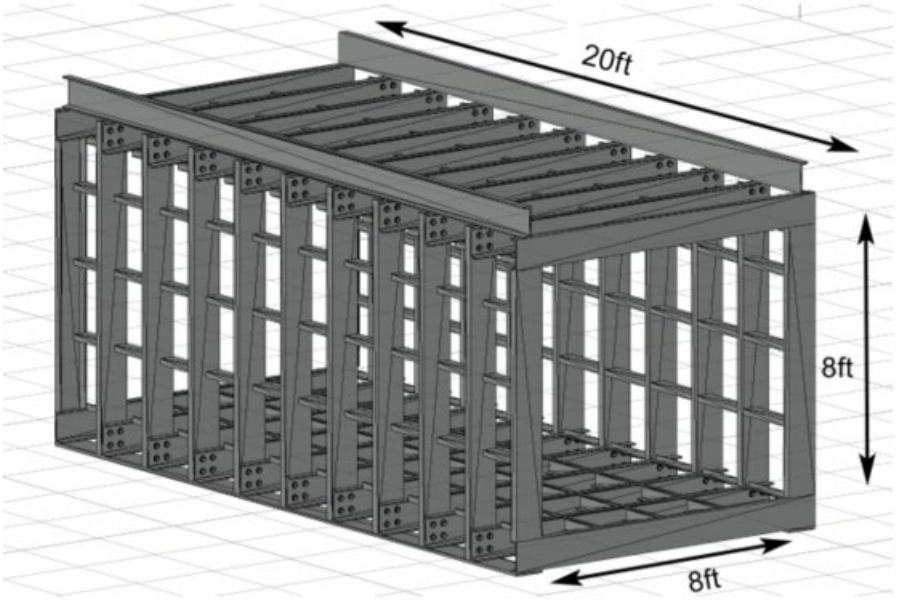

Figure 3-6: Large Shock Tube Design with Dimensions

The length of 40 feet was determined to be sufficient, as research has shown, the Kloppersbos research facility in South Africa utilizes a methane coal dust explosion tunnel of 10 meters (roughly 30 feet) to conduct testing of active barrier suppression systems. As mentioned previously, this length of shock tube does not allow for the explosion to transition from deflagration, into detonation, but still produces a significant explosion with a sizeable flame. Figure 3-7 below shows the fully constructed UKERT large shock tube.

Figure 3-7: Fully Constructed Large Shock Tube

3.1.8 Methane Concentration

Once again, it was necessary to plan for the highest potential explosion pressure, which occurs when the methane-air mixture is an ideal stoichiometric mixture. This occurs when the methane concentration is 9.5% methane by volume, which was the objective concentration. The methane entered the shock tube through a gas line in the closed end of the shock tube, and was controlled by a remote control ball valve. This can be seen at the bottom of Figure 3-9 (red gas line).

3.1.8.1 Mixing Fan

When the methane entered the large shock tube, it was mixed with air using a mechanical fan. The fan was constructed of wood and installed on the interior of the closed end of the shock tube where the methane-air mixture would occur. The fan measured 6 feet in diameter, and had panels that were 18 inches long and 12 inches long. The installed fan can be seen in Figure 3-8 below.

Figure 3-8: Mixing Fan From Interior of Shock Tube

The fan was controlled by a half horse power motor on the exterior of the closed-end of the shock tube. The mechanical system, as well as the methane gas inlet, can be seen in Figure 3-9 below.

Figure 3-9: Mixing Fan Mechanical Components from Exterior of Shock Tube

3.1.9 Membrane Material

It was crucial that the membrane material did not conduct static electricity, because static build up could lead to the chance of a spark, and a spark could ignite the methane mixture unexpectedly. Once again, the membrane material also needed to be thin enough so that it would rupture from the methane explosion. A velostat material with a thickness of 4 mil was used. The velostat came in a 54-inch width, so two pieces had to be taped together to cover the 8 foot by 8 foot cross sectional area. The membrane was placed 4 feet from the end of the shock tube. This provided a methane-air mixture volume of 256 ft^3, or 7.25 m^3. Figure 3-10 below shows the velostat membrane installed 4 feet from the closed end of the shock tube.

Figure 3-10: Installed Velostat Membrane

3.1.10 Gas Detectors

The same gas detectors utilized for the scaled shock tube were used for the large shock tube. Three MX6 iBRID gas detectors with infrared methane sensors were used to

monitor the methane concentration in the methane-air mixture zone of the large shock tube. Three holes were drilled in the side of the shock tube at two feet, four feet, and six feet from the floor level of the interior. Tubing attached to the pumps on the detectors were used to reach each of the holes. The test was not initiated until the methane detectors read an approximate stoichiometric concentration of methane, between 9 and 10 percent. Good mixing from the fan was observed, as the methane concentration on each gas detector increased at approximately the same rate. Figure 3-11 below shows the setup of the gas detectors outside of the shock tube, with their pump tubing installed in the appropriate hole.

Figure 3-11: MX6 iBRID Gas Detectors Setup

3.1.11 Igniters

Two electric matches were used to ignite the methane-air mixture in the large shock tube. These igniters were positioned on either side of the shock tube at two feet from the

closed-end and four feet from the floor level of the interior. The igniters were initiated at the same time. Once again, these igniters successfully ignited the methane-air mixture, allowing the explosion produced to rupture the velostat membrane. The location of one of the igniters can be seen in Figure 3-11 above (the yellow wire).

3.1.12 Pressure Sensors

The large shock tube had two PCB Piezotronic dynamic pressure sensors installed in the wall. The first was located 8 feet from the closed end of the shock tube, and 4 feet from the ground of the interior. The second was located 13 feet from the closed end of the shock tube, and also 4 feet from the ground of the interior. The pressure sensor closest to the membrane was rated for 200 psi, and the one farther from the membrane was rated for 50 psi. The experimental setup can be seen in Figure 3-12 below, with the locations of the igniters, membrane, and pressure sensors, and their designated channels.

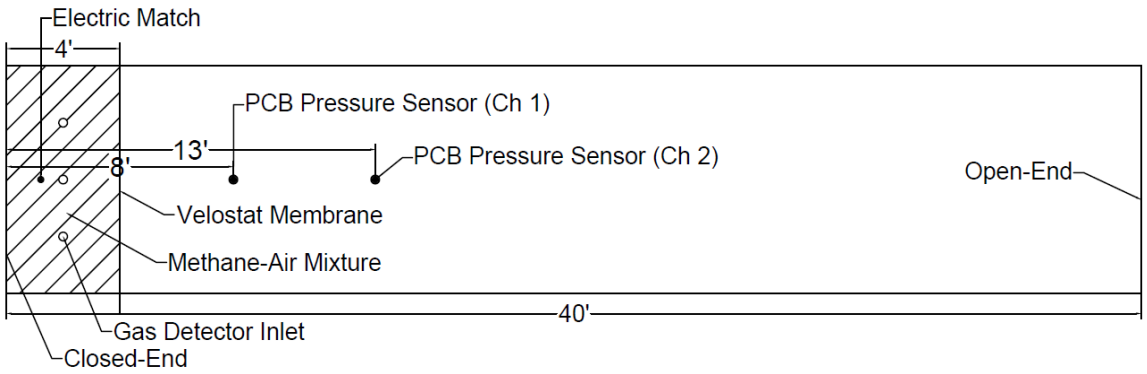

Figure 3-12: Large Shock Tube Experimental Setup

3.1.13 Data Acquisition Instrumentation

The same data acquisition system that was used for the scaled shock tube, was used to record the pressure sensor data for the large shock tube. The sensor located 8 feet from the closed-end of the shock tube utilized Channel 1, and the sensor located 13 feet from

the closed-end of the shock tube utilized Channel 2. The experimental results gathered from the methane explosion test in the large shock tube can be found in Chapter 4.

CHAPTER 4. EXPERIMENTAL RESULTS

Chapter 4 provides the experimental results from the methane explosion testing in the scaled shock tube, and the large shock tube. The pressure vs. time history at each pressure sensor is provided.

Scaled Shock Tube Experimental Results

As mentioned in Chapter 3, five PCB Piezotronic dynamic pressure sensors were installed in the scaled shock tube to gather the pressure vs. time history at designated points during a methane explosion. From the data gathered, the first three pressure sensors delivered useable data, and the last two did not. The pressure vs. time histories for the first three pressure sensors from this experiment are shown below in Figure 4-1, Figure 4-2, and Figure 4-3.

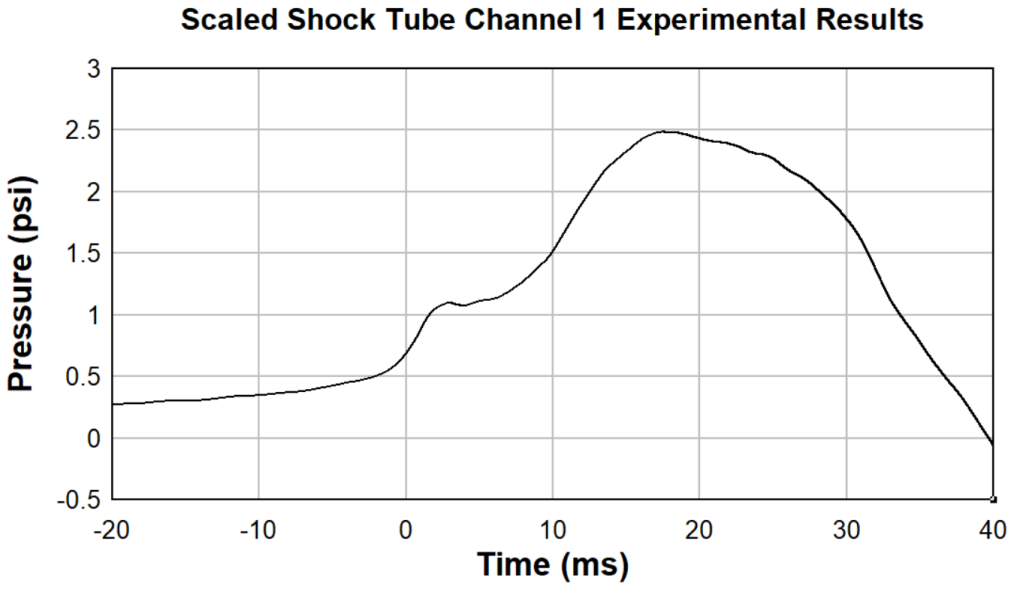

Figure 4-1: Scaled Shock Tube Channel 1 Experimental Pressure vs. Time History

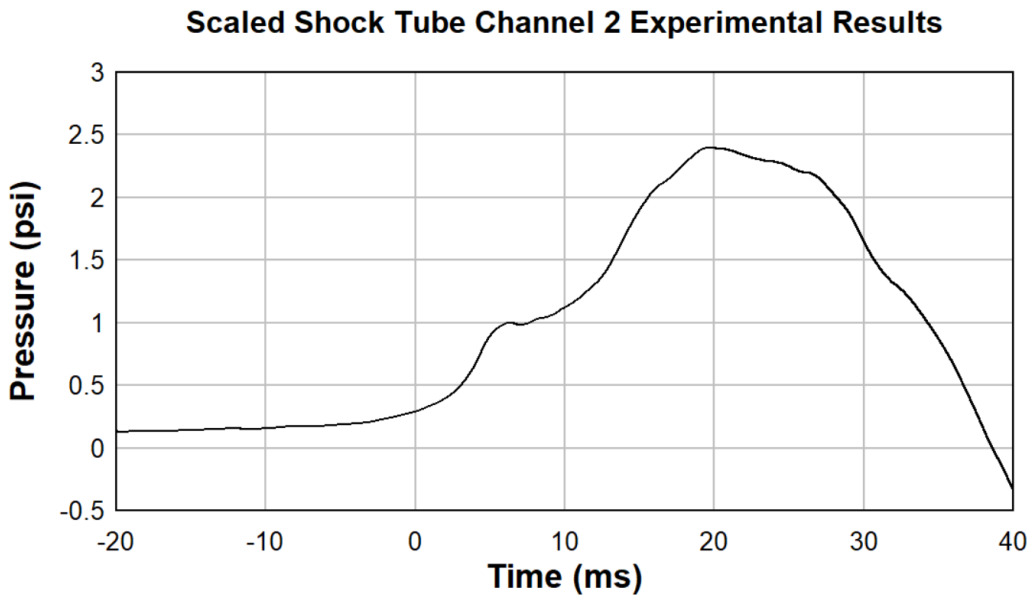

Figure 4-2: Scaled Shock Tube Channel 2 Experimental Pressure vs. Time History

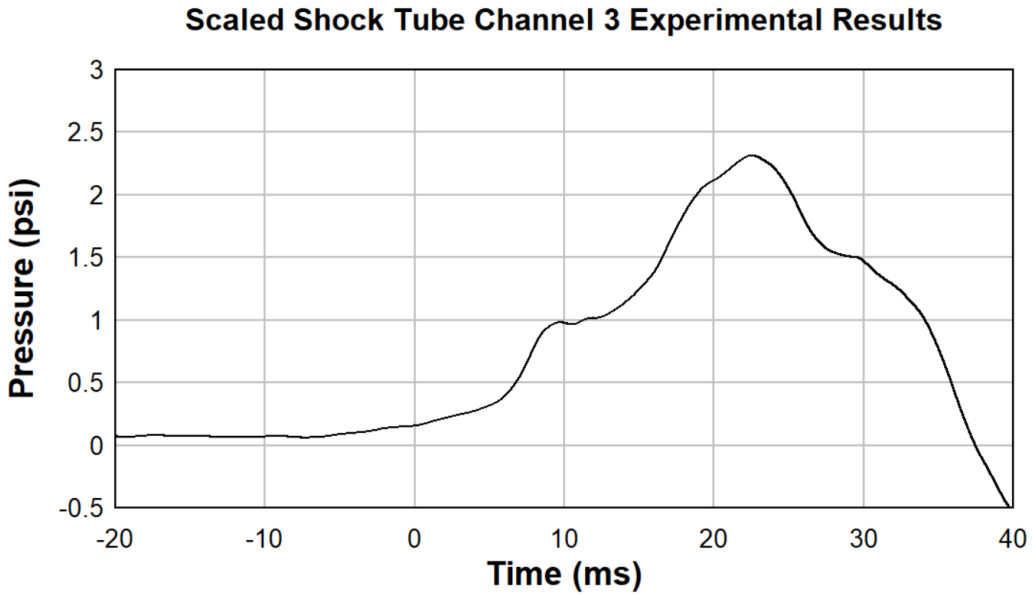

Figure 4-3: Scaled Shock Tube Channel 3 Experimental Pressure vs. Time History

The experimental results from the methane explosion in the scaled shock tube, shown above, have a noticeable initial pressure rise, followed by another pressure rise that

reaches the peak. This initial pressure rise, followed by the peak, could be attributed to the initial burst of the membrane, followed by the shock wave, the methane cloud being flash ignited, or the initial shock wave, followed by the reflected wave off the closed-end of the shock tube. Figure 4-4 below shows the combined pressure vs. time histories for all three pressure sensors.

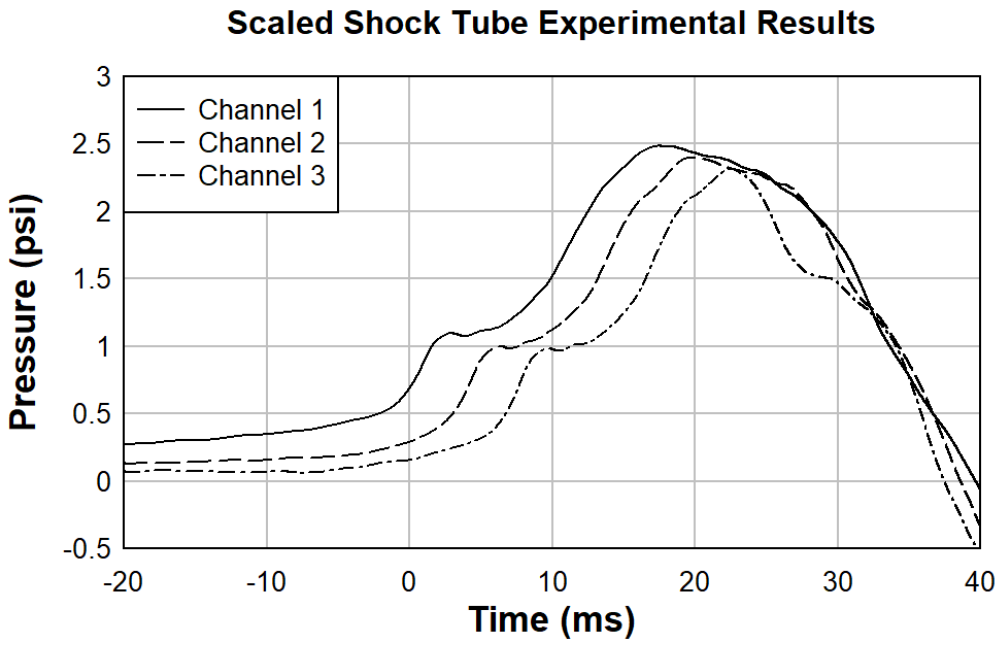

Figure 4-4: Scaled Shock Tube Combined Experimental Pressure vs. Time Histories

The peak pressure of the first pressure sensor (channel 1) was approximately 2.5 psi. The second and third pressure sensors (channels 2 and 3) reached approximate peaks of 2.4 psi and 2.3 psi respectively. This provided an almost perfectly linear decay in pressure. Also, the pressure curves leading up to the peaks followed the same shape, each offset by about 3 ms.

Large Shock Tube Experimental Results

As mentioned in Chapter 3, two PCB Piezotronic dynamic pressure sensors were installed in the large shock tube to gather the pressure vs. time history during a methane explosion. The pressure vs. time histories can be seen below in Figure 4-5 and Figure 4-6.

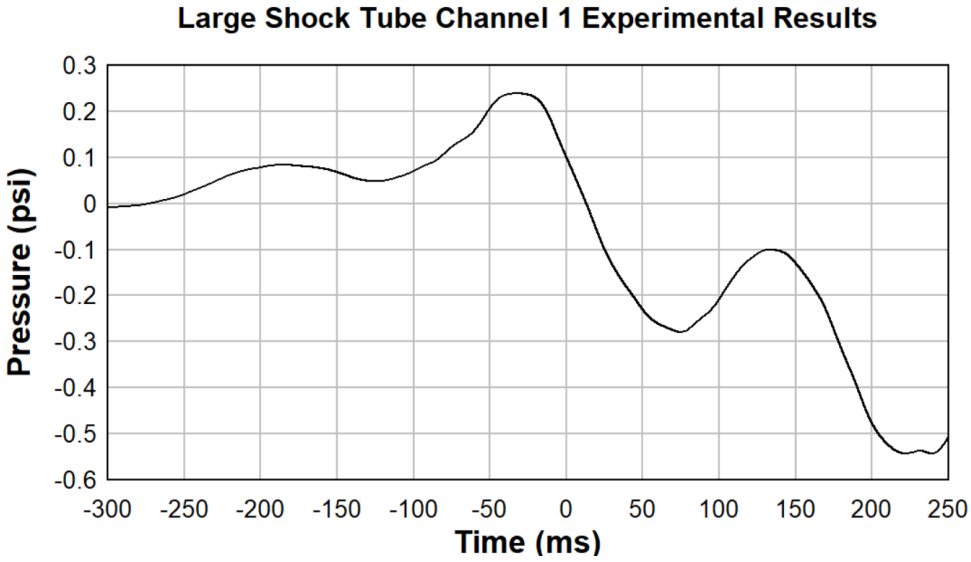

Figure 4-5: Large Shock Tube Channel 1 Experimental Pressure vs. Time History

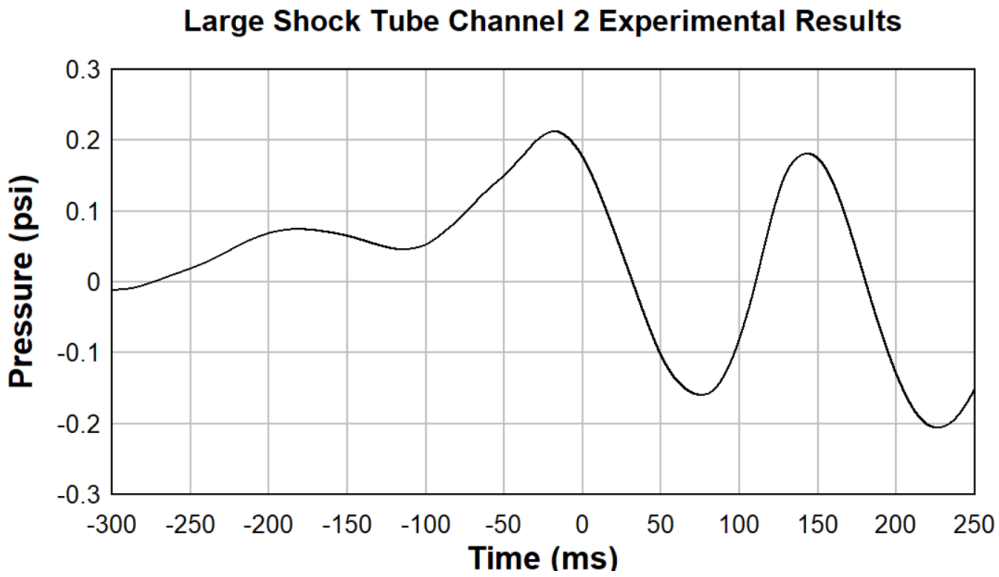

Figure 4-6: Large Shock Tube Channel 2 Experimental Pressure vs. Time History

Once again, there was an initial pressure rise, followed by another pressure rise that reached the peak. The first pressure sensor (channel 1) reached a peak pressure of approximately 0.24 psi, and the second pressure sensor (channel 2) reached a peak pressure of approximately 0.22 psi. Also, it should be noted that the pressure rise for both sensors began before 0 ms, however, the timing was solely dependent on the time at which the DataTrap chooses to trigger. Figure 4-7 below shows the combined pressure vs. time histories for both pressure sensors.

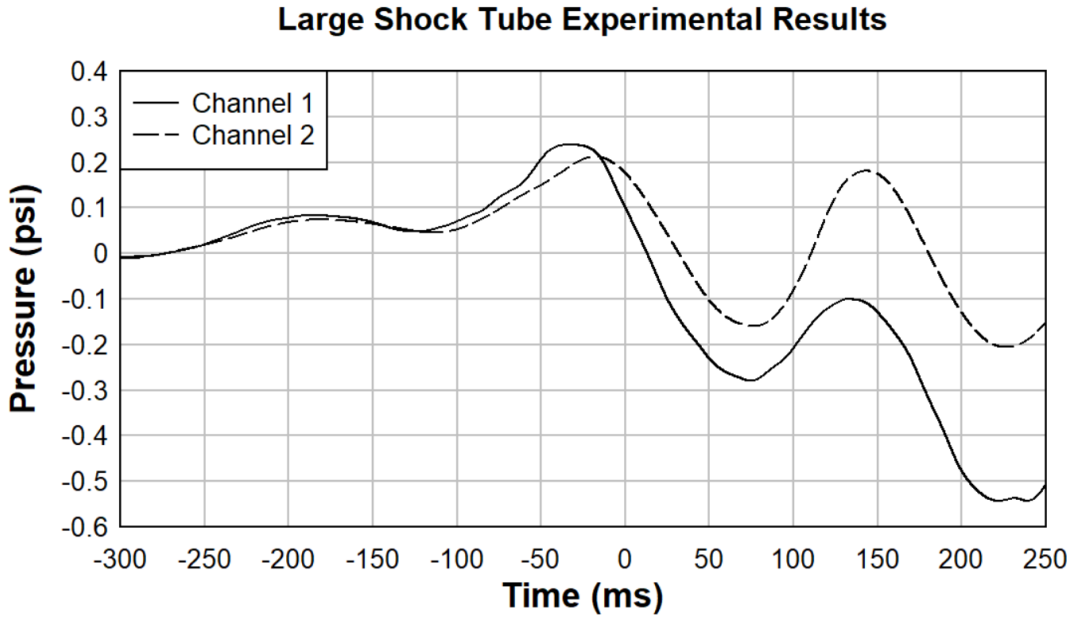

Figure 4-7: Large Shock Tube Combined Experimental Pressure vs. Time Histories

The pressure rise of both sensors followed the same shape. There is only a significant offset between the curves near the peaks, and after the peaks.

CHAPTER 5. CFD MODELING SETUP

Chapter 5 outlines the CFD modeling setup in SC/Tetra for each of the three case studies. The first models the combustion of methane, the second models a methane explosion using a total pressure boundary condition at the location of the membrane, and the third models a large scale methane explosion using the bursting balloon CFD technique.

Case Study 1: Combustion of Methane

5.1.1 3D Model Creation

The 3D model for the first case study represented a slice of the center of the scaled shock tube, in order to reduce run-time. The pressure sensors and ignition source were located in this slice. The model was made up of three closed volumes, the methane-air mixture behind the membrane, the ignition source, and the shock tube air on the other side of the membrane. The fluid assigned to all three volume regions was compressible air. The model dimensions were 0.4 inches by 11 inches, by 11.5 feet. The entire length of the shock tube was not modeled since pressure sensors four and five did not provide acceptable data. The model also had five surface regions distinguishing the walls (top and bottom of shock tube), the methane-air mixture inlet, the shock tube outlet, the ignition source, and the planes on the sides of the model, making the slice. A diagram of the model can be seen in Figure 5-1 below.

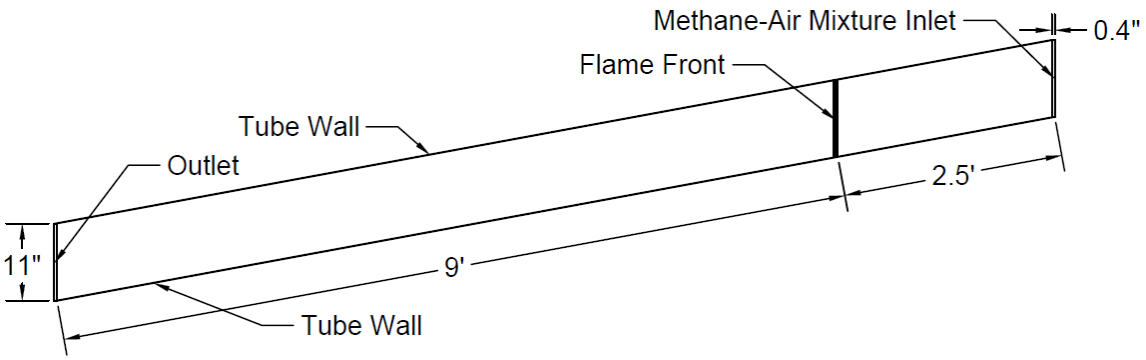

Figure 5-1: Case Study 1 3D Model Dimensions and Surface Regions

5.1.2 Analysis Types

The analysis type was turbulent flow, utilizing the RANS equations, and the standard k-ε turbulence model. The temperature was solved for since combustion was being solved for and the working fluid was compressible. Additionally, ten (10) diffusive species were solved for, as well as chemical reactions.

5.1.3 Basic Settings

This was a transient simulation with the courant number set to 1, indicating that the fluid particles move from one cell to another within one time step, and the initial time step set to 1 e-06 seconds. 600 cycles were used to gather the necessary data. Also, the force of gravity was applied at -32.3 ft/s^2 in the Y direction.

5.1.4 Material Properties

As mentioned previously, the fluid was compressible air. It was also a mixing gas and utilized the universal gas constant of 8.31451 J/mol K.

5.1.5 Diffusion

The diffusion coefficients of multi-component gas mixtures were set. The values for characteristic length, characteristic temperature, and DELT were entered for each species. DELT was a dimensionless constant representing the polarity of the molecule in the improved stockmayer potential. In order to define effective diffusion coefficients, the option to regard the binary diffusion coefficients with the species of the last index (e.g., carrier gas) as effective diffusivities was selected. The values summarized in Table 5-1 below were entered for characteristic length, characteristic temperature, and DELT for each species.

Table 5-1: Diffusion Coefficients of Multi-Component Gas Mixture

Species No	**Species**	**Characteristic Length (0.1 nm)**	**Characteristic Temperature (K)**	**DELT (-)**
1	CH_4	3.746	141	0
2	O_2	3.458	107.4	0
3	H_2O	2.605	572.4	1.217
4	N_2	3.621	97.53	0
5	CO_2	3.763	244	0
6	O	2.75	80	0
7	N	3.298	71.4	0
8	NO	3.621	97.53	0
9	OH	2.75	80	0
10	H	2.05	145	0

The parameters for heat of formation, molar mass, viscosity, specific heat, and thermal conductivity were also set. The values are summarized in Table 5-2 below.

Table 5-2: Diffusion Properties of Species

Species	Heat Generation (J/kg)	Molar Mass (kg/mol)	Viscosity (Pa-s)	Specific Heat (J/(kgK))	Thermal Conductivity (W/(m K))
CH4	-4667020	0.016043	5.02E-05	5830	4.15E-01
O2	0	0.031998	8.91E-05	1228	4.15E-01
H2O	-13434778	0.018	8.26E-05	2933	4.15E-01
N2	0	0.0280134	7.50E-05	1286	4.15E-01
CO2	-8941853	0.044	7.63E-05	1363	4.15E-01
O	15574290	0.015999	9.33E-05	1315	4.15E-01
N	33746710	0.0140067	9.32E-05	1560	4.15E-01
NO	3009128	0.0300057	8.19E-05	1219	4.15E-01
OH	2289469	0.017	8.09E-05	2104	4.15E-01
H	216268800	0.001	3.16E-05	18228	4.15E-01

5.1.6 Initial Conditions

Several initial conditions were set for pressure, temperature, and species concentration. The concentration of diffusive species 1 (CH_4) for the methane-air mixture was ensured to be 0.095, or 9.5%, the ideal stoichiometric concentration. Additionally, the temperature of the ignition source volume was set to 1112℉ (600℃), which is slightly higher than the auto-ignition temperature of methane (1076℉ or 580℃) (Fuels and Chemicals - Auto Ignition Temperature, 2003). The initial conditions are summarized in Table 5-3 below.

Table 5-3: Initial Conditions

Variable	Value	Region
Pressure	0 psi	All
Temperature	1112℉	Ignition Source
Temperature	80℉	Methane-Air-Mixture & Shock Tube Air
Concentration of diffusive species (1)	0.095	Methane-Air Mixture
Concentration of diffusive species (2)	0	Methane-Air Mixture
Concentration of diffusive species (3)	0	Methane-Air Mixture
Concentration of diffusive species (4)	0.905	Methane-Air Mixture
Concentration of diffusive species (1)	0	Ignition Source
Concentration of diffusive species (2)	0	Ignition Source
Concentration of diffusive species (3)	0.01	Ignition Source
Concentration of diffusive species (4)	0.99	Ignition Source
Concentration of diffusive species (1)	0	Shock Tube Air
Concentration of diffusive species (2)	0.23184	Shock Tube Air
Concentration of diffusive species (3)	0	Shock Tube Air
Concentration of diffusive species (4)	0.76816	Shock Tube Air

5.1.7 Boundary Conditions

Three boundary conditions were applied to the model. The shock tube walls were assigned the wall conditions of free slip and adiabatic. The outlet, which was the open end of the shock tube, was assigned a natural inflow/outflow condition. Lastly, an inflow velocity of 95 ft/s (29 m/s) was assigned acting normal to the surface of the methane-air mixture inlet.

5.1.8 Chemical Reactions

There were 7 chemical reactions to consider, 1 pre-mixed combustion, and 6 Arrhenius equations. The pre-mixed combustion equation can be seen below, followed by the Arrhenius type equations.

$$CH_4 + 2O_2 \rightarrow CO_2 + 2H_2O \tag{8}$$

$$N_2 + O \leftrightarrow NO + N \quad (9)$$

$$N + O_2 \leftrightarrow NO + O \quad (10)$$

$$N + OH \leftrightarrow NO + H \quad (11)$$

Additionally, the variable values for the reaction rate in the format of equation 12 below were input.

$$k = AT^n \exp(\frac{-Ea}{RT}) \quad (12)$$

Table 5-4 below displays these inputs for the six Arrhenius equations.

Table 5-4: Reaction Rate Variables

k	**A**	**Ea/R**
k_2	1.8 x 10^8	exp(-38730/T)
k_{-2}	3.8 x 10^7	exp(-425/T)
k_3	1.8 x 10^4	exp(-4680/T)
k_{-3}	3.8 x 10^3	exp(-20820/T)
k_4	7.1 x 10^7	exp(-450/T)
k_{-4}	1.7 x 10^8	exp(-24560/T)

5.1.9 Solver Settings

For the matrix solver, a relative error of 1 e-06 was set for all equations. Additionally, for variables U, V, W, k and ε, the maximum iterations was set to 100. For pressure (P), and temperature (T), the maximum iterations set to 500. Finally, for all species the maximum iterations was set to 200.

The pressure correction method used was the Modified SIMPLEC Method. The number of iteration loops in a cycle was limited to 10. Lastly, the accuracy of the time derivative terms was set to the second-order implicit scheme.

5.1.10 Output Control

A time series output control was used to output specified variables at arbitrary coordinates to a csv file. The three locations of the pressure sensors that provided acceptable data were input, and the series was set to output the pressure values every cycle.

5.1.11 Octree/Mesh Creation

To create the octree, (the volume that contains the model) a minimum octant size value was entered as 0.2 inches (0.005 meters). The octree was comprised of 416,988 elements at one level of refinement, meaning all elements were the same size. Reducing the mesh size did not significantly change the results, and only increased the run-time, therefore the mesh was determined to be sufficient. A cross section of the octree along the slice of the shock tube can be seen in Figure 5-2 below.

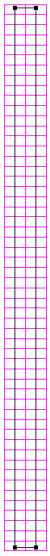

Figure 5-2: Case Study 1 Cross Section of Octree

Using the octree created, and surface and volume mesh was generated. The mesh contained 501,181 elements. The mesh was made up of tetrahedrons. A cross section of the mesh along the slice of the shock tube can be seen in Figure 5-3 below.

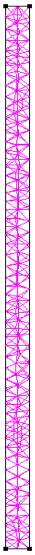

Figure 5-3: Case Study 1 Cross Section of Mesh

Once the mesh for the model was created, the solver was run, taking approximately 16 hours to reach the final designated cycle. This was sufficient in providing the initial peak pressure at each pressure sensor location. The numerical pressure data at each of the three pressure sensor points was recorded in a csv file, as described above, and used in Chapter 6, Numerical Results.

Case Study 2: Total Pressure Boundary Condition

5.1.12 3D Model Creation

The 3D model for the second case study was made up of one closed volume, which represented the scaled shock tube from the membrane to the open end. The model dimensions were 10.875 inches by 11 inches, and 18 feet long. The model had one volume

region and three surface regions. The volume region represented the air within the scaled shock tube. The fluid assigned to this region was compressible air. The three surface regions distinguished the tube walls, membrane, and outlet, and can be seen in Figure 5-4 below.

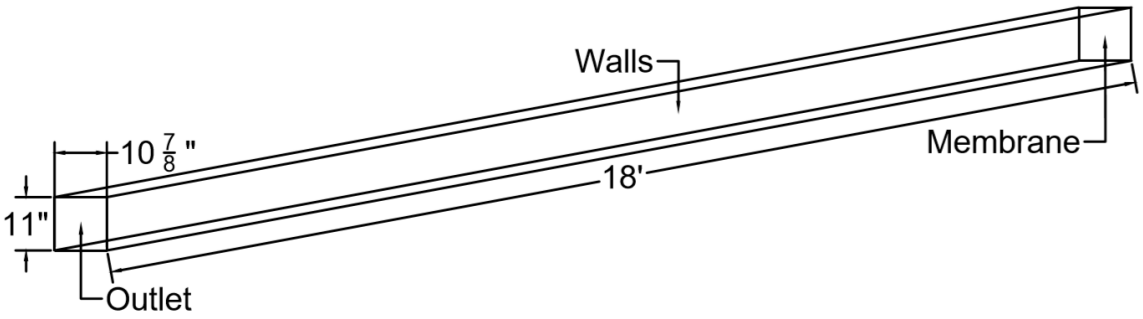

Figure 5-4: Case Study 2 3D Model Dimensions and Surface Regions

5.1.13 Analysis Conditions

The analysis type was turbulent flow, utilizing the RANS equations, and the standard k-ε turbulence model. Additionally, the temperature was solved for. An initial condition of 80℉ (26. 85℃) was set for the air in the shock tube. This was a transient simulation with the courant number set to 1, and the initial time step set to 1 e-05 seconds. 1300 cycles were used to gather the necessary data. The full consumption of the fuel in the ignited methane zone was assumed. Therefore, the shock wave propagated in a non-reactive environment, and chemical reactions did not need to be considered.

Boundary conditions were set for each of the surface regions. The shock tube walls were assigned the wall conditions of free slip and adiabatic. The outlet, which was the open end of the shock tube, was assigned a natural inflow/outflow condition. Finally, the membrane utilized a total pressure boundary condition which allowed a table input of a

total pressure vs. time curve that would be exerted perpendicular to the membrane boundary. Table 5-5 below displays the table input of the total pressure vs. time curve.

Table 5-5: Total Pressure vs. Time Input Values

Time (ms)	Pressure (psi)
0	1.102
4	1.102
8	1.305
14	2.393
15	2.393
17	2.611
20	2.611
23	2.538
27	2.321
45	0

The software used linear interpolation between the input points to create the curve. The curve can be seen in Figure 5-5 below.

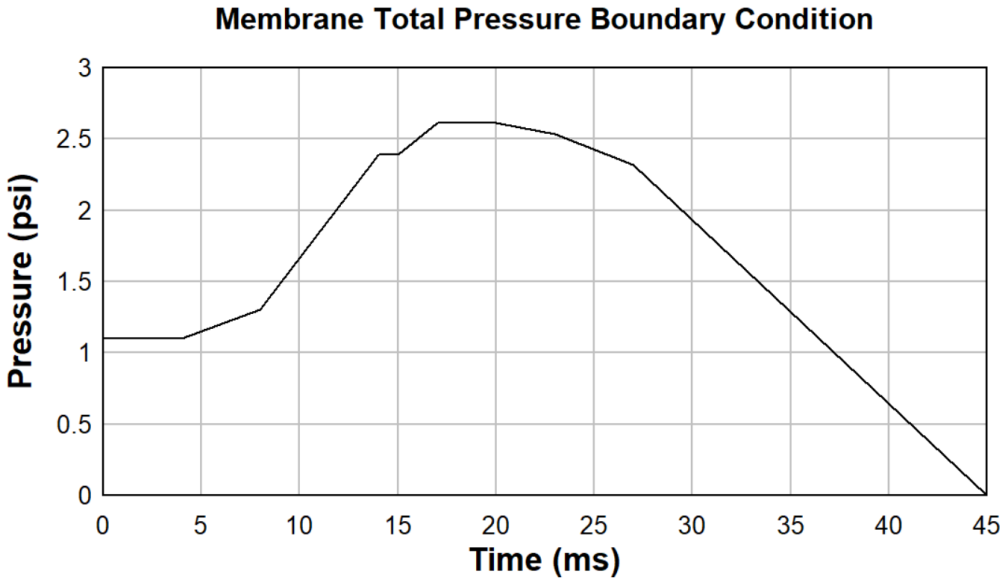

Figure 5-5: Linear Interpolation of Total Pressure vs. Time Curve

This curve did not replicate the pressure vs. time curve recorded by the pressure sensors. It provided the appropriate pressure peaks and durations to allow for the recreation of the recorded pressure vs. time curves at their specified locations. The peak pressures of the curve were slightly higher than the recorded peak pressures to account for pressure losses.

The final analysis condition was a time series condition which output specified variables at arbitrary coordinates to a csv file. The three locations of the pressure sensors that provided acceptable data were input, and the series was set to output the pressure values every cycle.

5.1.14 Octree/Mesh Creation

The creation of the mesh was quite simple. The 3D model was not complex. Therefore, the mesh did not need to be. A minimum octant size value was entered as 0.39 inches (0.01 meters), and the octree was created. The octree was comprised of 531,020 elements at three levels of refinement, 1.57, 0.79, and 0.39 inches (0.04, 0.02, and 0.01 meters). The smallest elements were closest to the walls, and the largest elements were closest to the center of the shock tube. Reducing the mesh size did not significantly change the results, and only increased the run-time. Therefore, the mesh was determined to be sufficient. A cross section of the octree along the shock tube can be seen in Figure 5-6 below.

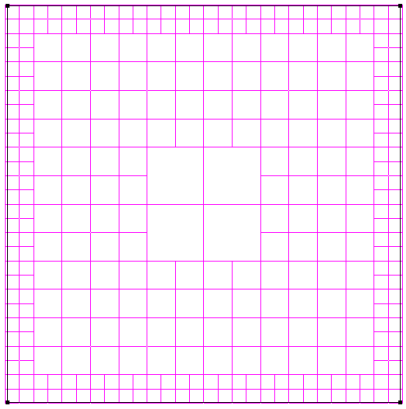

Figure 5-6 Case Study 2 Cross Section of Octree

Using the octree created, the surface and volume mesh was generated. The mesh contained 598,897 elements. The mesh was made up of tetrahedrons. A cross section of the mesh along the shock tube can be seen in Figure 5-7 below.

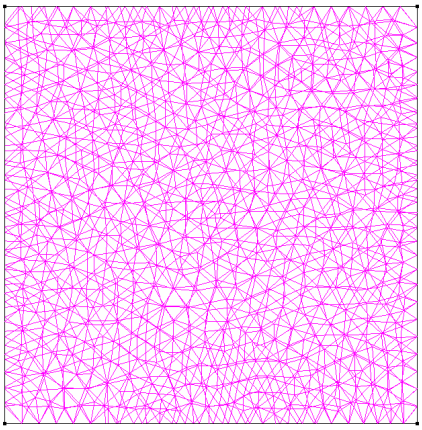

Figure 5-7: Case Study 2 Cross Section of Mesh

Once the mesh for the model was created, the solver was ran, taking approximately 40 minutes to reach the final designated cycle. The numerical pressure data at each of the three pressure sensor points was recorded in a csv file, as described above, and used in Chapter 6, Numerical Results.

Case Study 3: Bursting Balloon Technique

5.1.15 3D Model Creation

The 3D model for the third case study was made up of two closed volumes, which represented the methane-air mixture behind the membrane, and the area of the shock tube past the membrane. The entire length of the large shock tube did not need to be modeled for validation because there were no pressure sensors past 13 feet from the closed end. The model dimensions were 8 feet, by 8 feet, by 13.5 feet. The fluid assigned to both regions was compressible air. There were three surface regions, distinguishing the tube walls, membrane, and outlet, and can be seen in Figure 5-8 below.

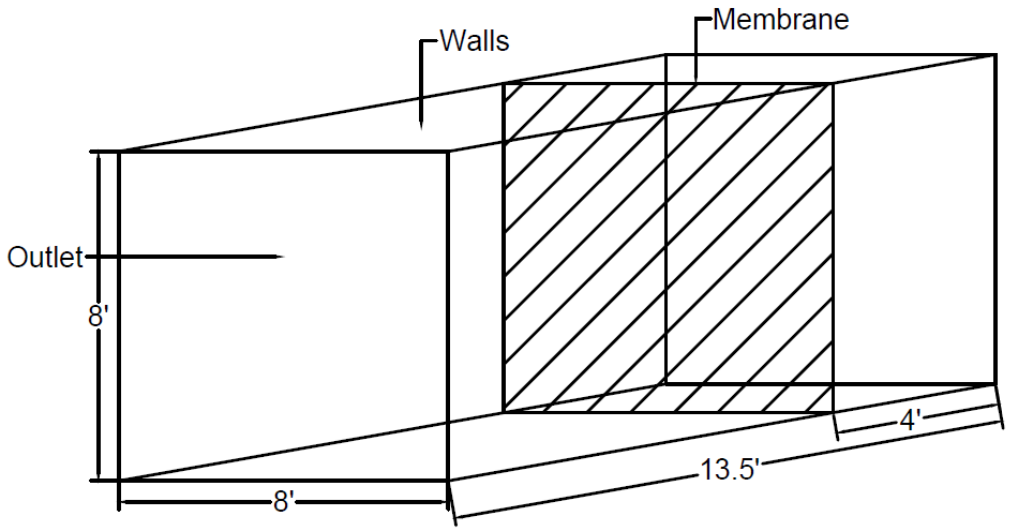

Figure 5-8: Case Study 3 3D Model Dimensions and Surface Regions

5.1.16 Analysis Conditions

The analysis type was turbulent flow, utilizing the RANS equations, and the standard k-ε turbulence model. Additionally, temperature was solved for. This was a transient simulation with the courant number set to 1, and the initial time step set to 1 e-03 seconds. 200 cycles were used to gather the necessary data. The full consumption of the fuel in the

ignited methane zone was assumed. Therefore, the shock wave propagated in a non-reactive environment, and chemical reactions did not need to be considered.

Two initial temperature conditions were applied; a temperature of 80℉ (26.85℃) was set for the air in the shock tube, and a temperature of 400℉ (204℃) was set for the methane-air mixture. An initial pressure condition of 0.36 psi, and an initial velocity condition of 311 ft/s (95 m/s) was applied to the methane-air mixture. Additionally, the initial pressure of the air in the shock tube was set to 0 psi.

Boundary conditions were set for the walls and outlet surface regions. The shock tube walls were assigned the wall conditions of free slip and adiabatic. The outlet, which was the open end of the shock tube, was assigned a natural inflow/outflow condition.

The final analysis condition was a time series condition which output specified variables at arbitrary coordinates to a csv file. The two locations of the pressure sensors were input, and the series was set to output the pressure values every cycle.

5.1.17 Octree/Mesh Creation

Once again, the octree creation was simple, as the 3D model was not complex. A minimum octant size was entered as 1.97 inches (0.05 meters), and the octree was created. The octree was comprised of 182,444 elements at three levels of refinement, 7.87, 3.94, and 1.97 inches (0.2, 0.1, and 0.05 meters). The smallest elements were closest to the walls, and the largest elements were closest to the center of the shock tube. Reducing the mesh size did not significantly change the results, and only increased the run-time. Therefore, the mesh was determined to be sufficient. A cross section of the octree along the shock tube can be seen in Figure 5-9 below.

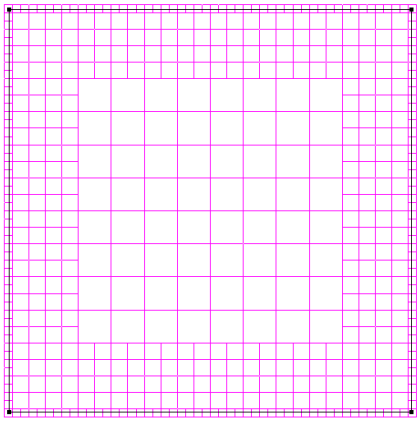

Figure 5-9: Case Study 3 Cross Section of Octree

Using the octree created, the surface and volume mesh was generated. The mesh contained 180,256 elements. The mesh was made up of tetrahedrons. A cross section of the mesh along the shock tube can be seen in Figure 5-10 below.

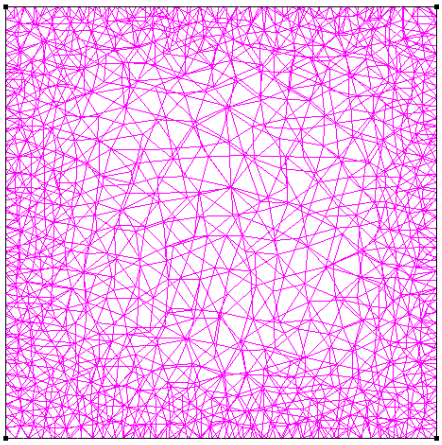

Figure 5-10: Case Study 3 Cross Section of Mesh

Once the mesh for the model was created, the solver was ran, taking approximately 20 minutes to reach the final designated cycle. The numerical pressure data at each of the pressure sensor points was recorded in a csv file, as described above, and used in Chapter 6, Numerical Results.

CHAPTER 6. NUMERICAL RESULTS

Chapter 6 provides the results of each CFD simulation for the three case studies. The first two case studies used three pressure sensor data points for validation, and the third used two pressure sensor data points for validation.

Case Study 1 Numerical Results

The numerical results for the first case study had some limitations due to the model run-time. Noticeably, the pressure vs. time curves are not complete, but they do reach their peak pressures. This was determined to be sufficient information for comparison of the model at this time. The pressure vs. time curve for the first pressure sensor location (channel 1) in the scaled shock tube for the combustion of methane model can be seen below in Figure 6-1.

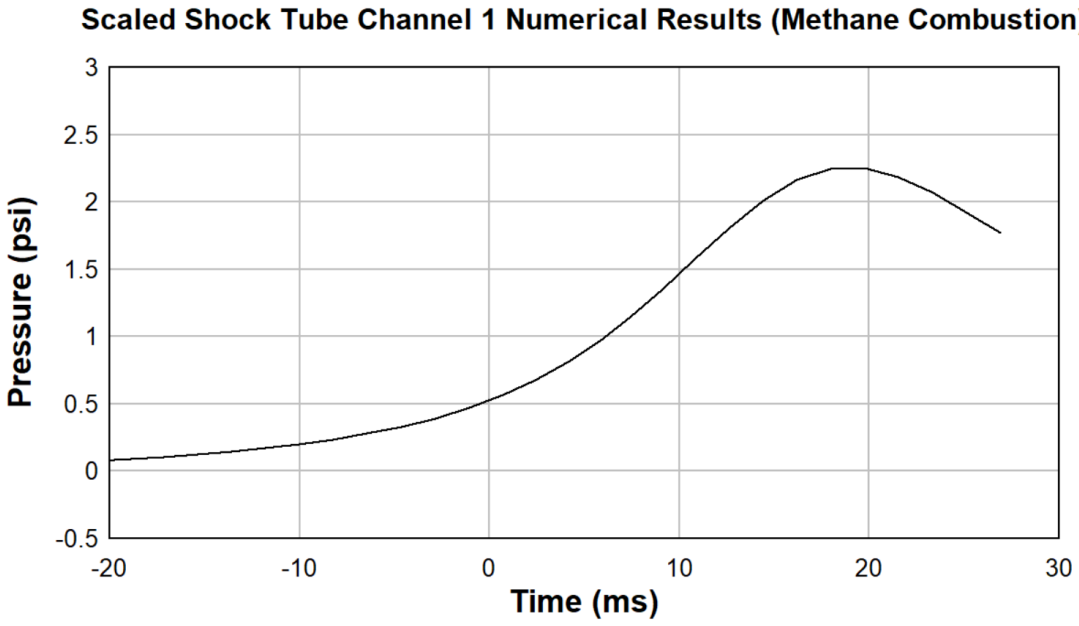

Figure 6-1: Case Study 1 Channel 1 Numerical Results

The timing of the initial pressure rise had to be calibrated with the experimental data. As mentioned previously, the recorded pressure rise can begin before 0 ms, because the timing of the experimental results is solely dependent on the time at which the DataTrap chooses to trigger.

When compared with the experimental results, the pressure rise of the curve is in good agreement. However, there is no distinguished initial pressure rise prior to the pressure rise that reaches the peak. This could be attributed to the model not accounting for the membrane burst. The pressure peaks are also in good agreement. The experimental results reached a peak pressure of 2.49 psi at 17.46 ms, and the numerical results reached a peak pressure of 2.25 psi at 17.96 ms. The comparison of results for case study 1, channel 1, can be seen below in Figure 6-2.

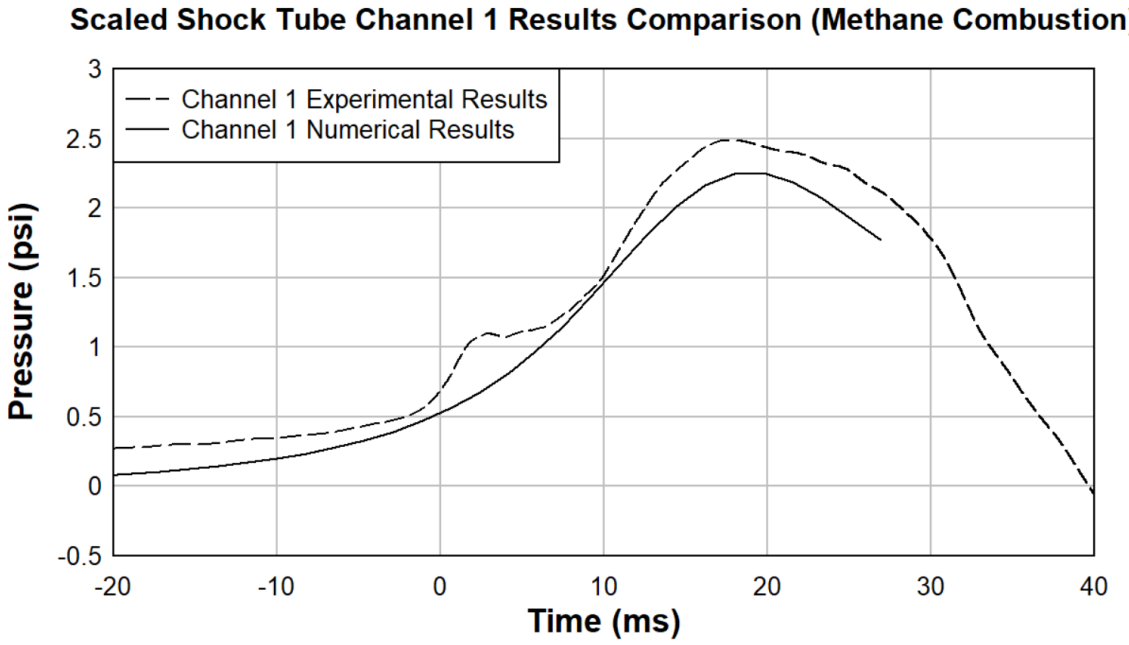

Figure 6-2: Case Study 1 Channel 1 Results Comparison

The pressure vs. time curve for the second pressure sensor location (channel 2) in the scaled shock tube for the combustion of methane model can be seen below in Figure 6-3.

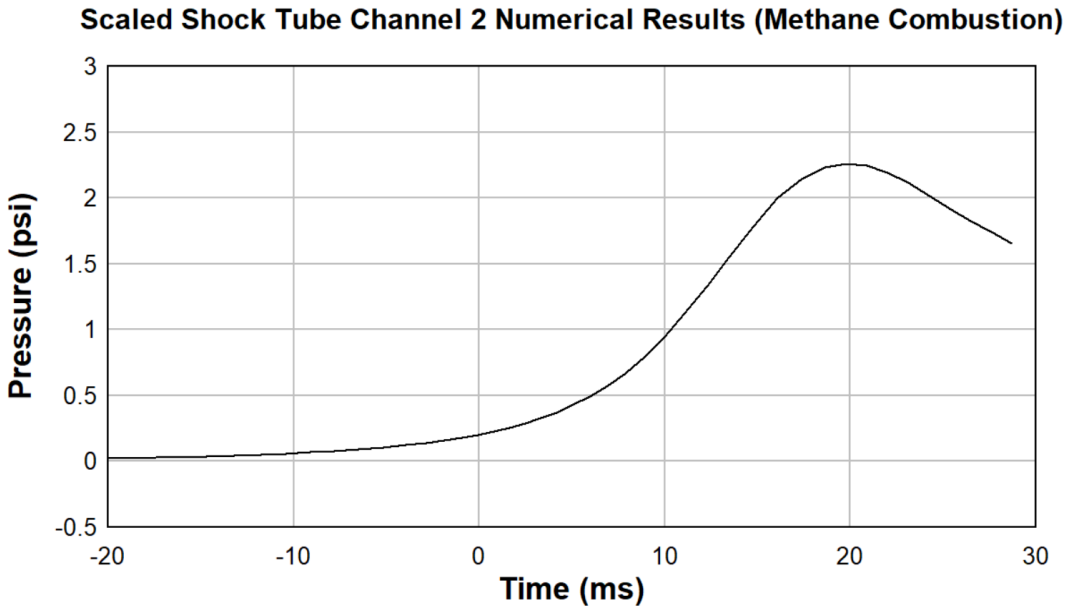

Figure 6-3: Case Study 1 Channel 2 Numerical Results

When compared with the experimental results, the pressure rise of the curve is in good agreement. Again, there is no initial pressure rise prior to the pressure rise that reaches the peak. The peak pressures are also in good agreement. The experimental results reached a peak pressure of 2.40 psi at 19.58 ms, and the numerical results reached a peak pressure of 2.26 psi at 19.77 ms. The comparison of results for case study 1, channel 2, can be seen below in Figure 6-4.

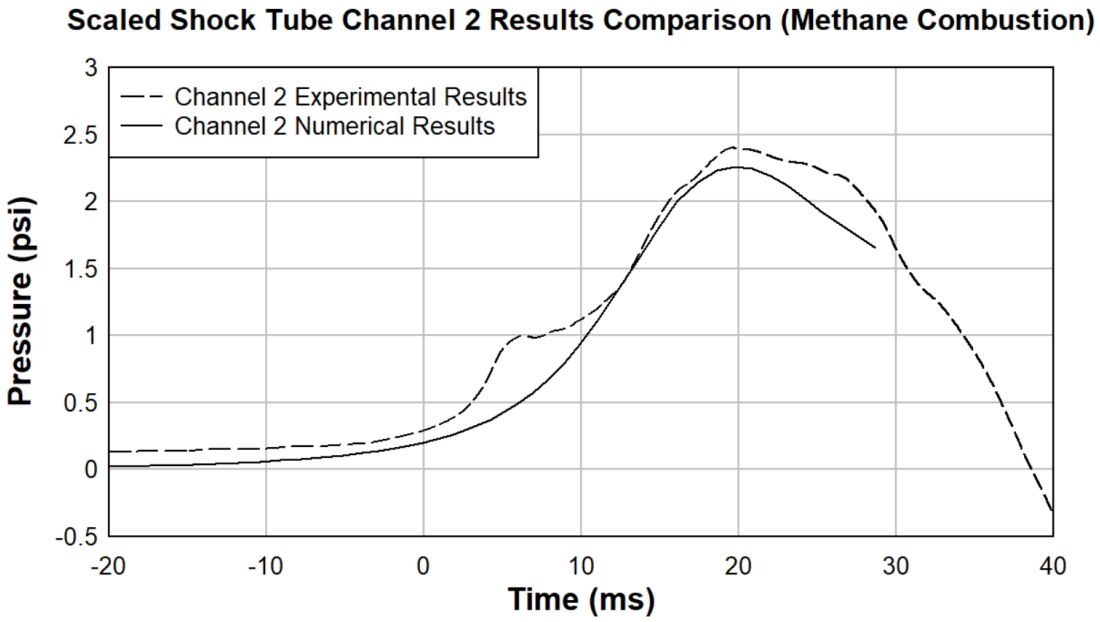

Figure 6-4: Case Study 1 Channel 2 Results Comparison

The pressure vs. time curve for the third pressure sensor location (channel 3) in the scaled shock tube for the combustion of methane model can be seen below in Figure 6-5.

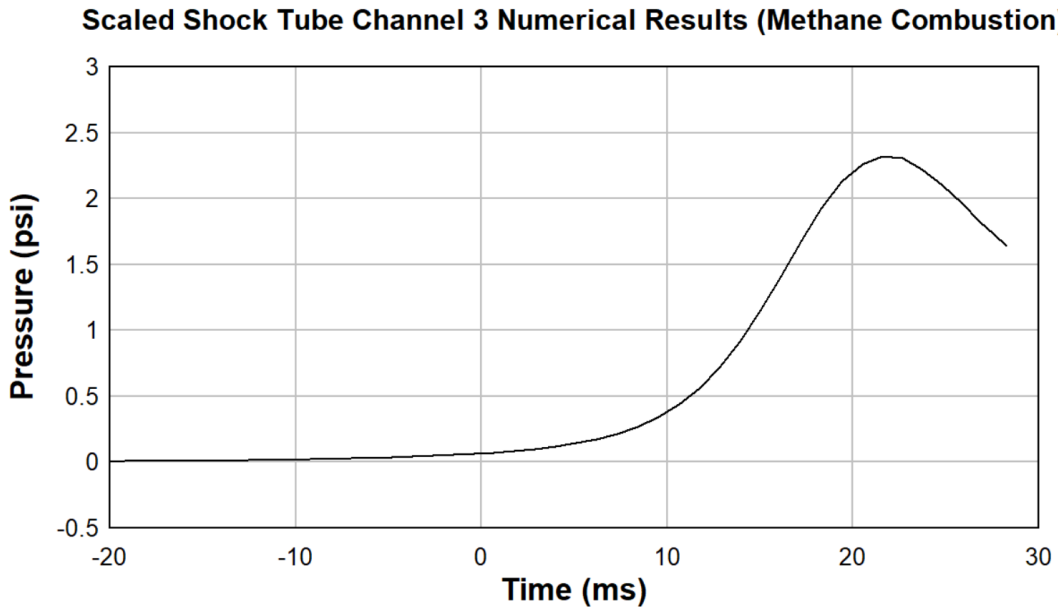

Figure 6-5: Case Study 1 Channel 3 Numerical Results

When compared with the experimental results, the pressure rise of the curve is in good agreement. Once again, there is no initial pressure rise before the pressure rise that reaches the peak. The peak pressures are also in good agreement. The experimental results reached a peak pressure of 2.31 psi at 22.51 ms, and the numerical results reached a peak pressure of 2.32 psi at 21. 57 ms. The comparison of results for case study 1, channel 3, can be seen below in Figure 6-6.

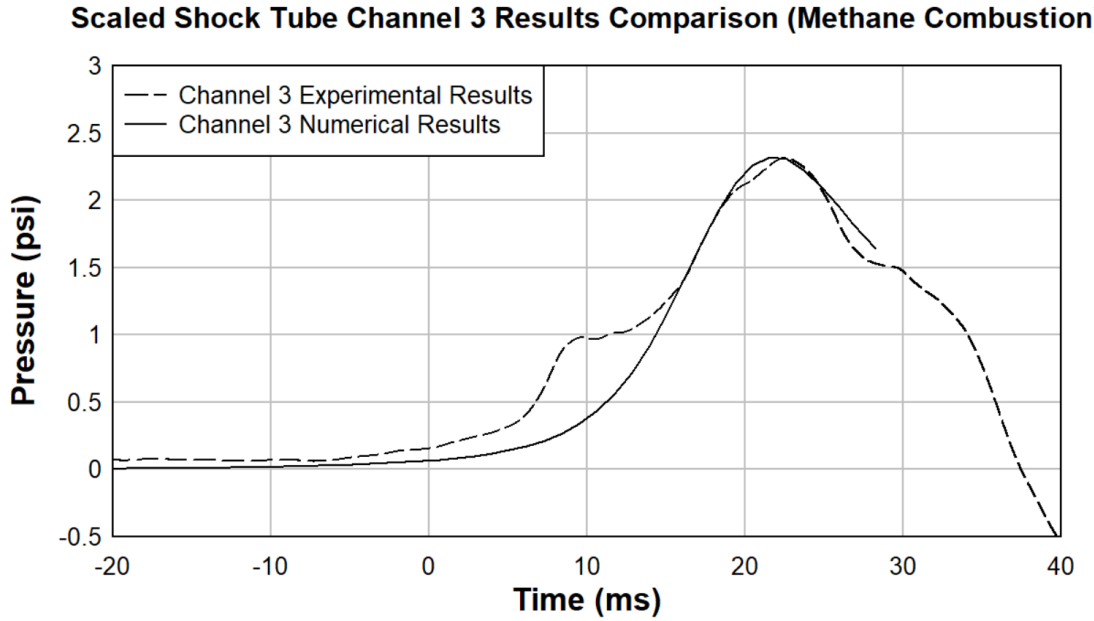

Figure 6-6: Case Study 1 Channel 3 Results Comparison

Case Study 2 Numerical Results

The pressure vs. time curve for the first pressure sensor location (channel 1) in the scaled shock tube for the total pressure boundary condition model can be seen below in Figure 6-7.

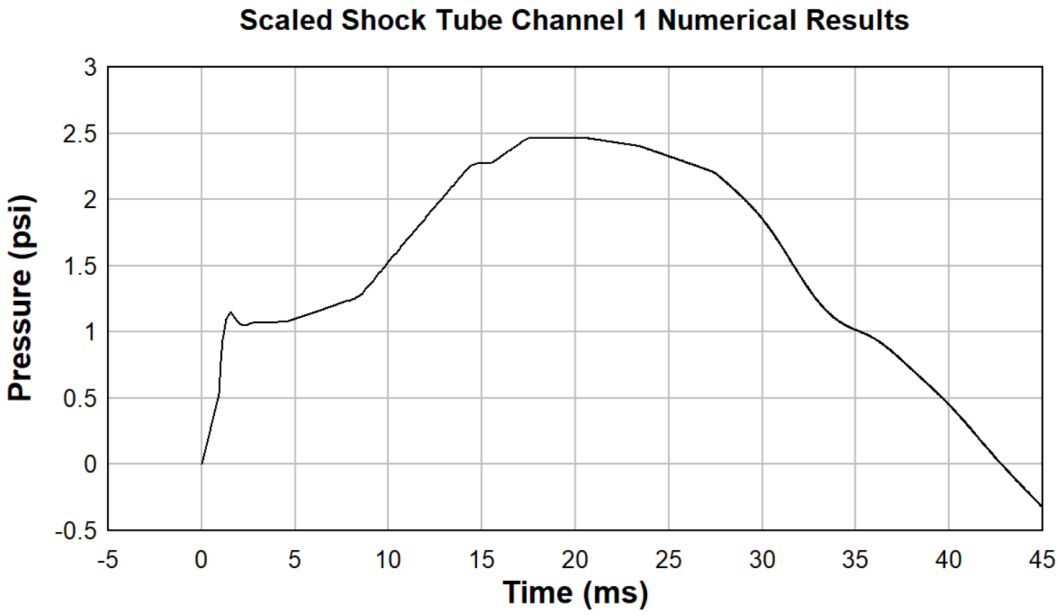

Figure 6-7: Case Study 2 Channel 1 Numerical Results

The numerical results are in excellent agreement with the experimental results. While there is not a slow initial pressure rise, as seen in the experimental results, there are two distinctive pressure rises, an initial one, and one that reaches the peak. Additionally, the duration of the curve is accurate, and no timing adjustment was necessary for this case study. The peak pressures are also in excellent agreement. The experimental results reached a peak pressure of 2.49 psi at 17.46 ms, and the numerical results reached a peak pressure of 2.47 psi at 17.75 ms. The comparison of results for case study 2, channel 1, can be seen below in Figure 6-8.

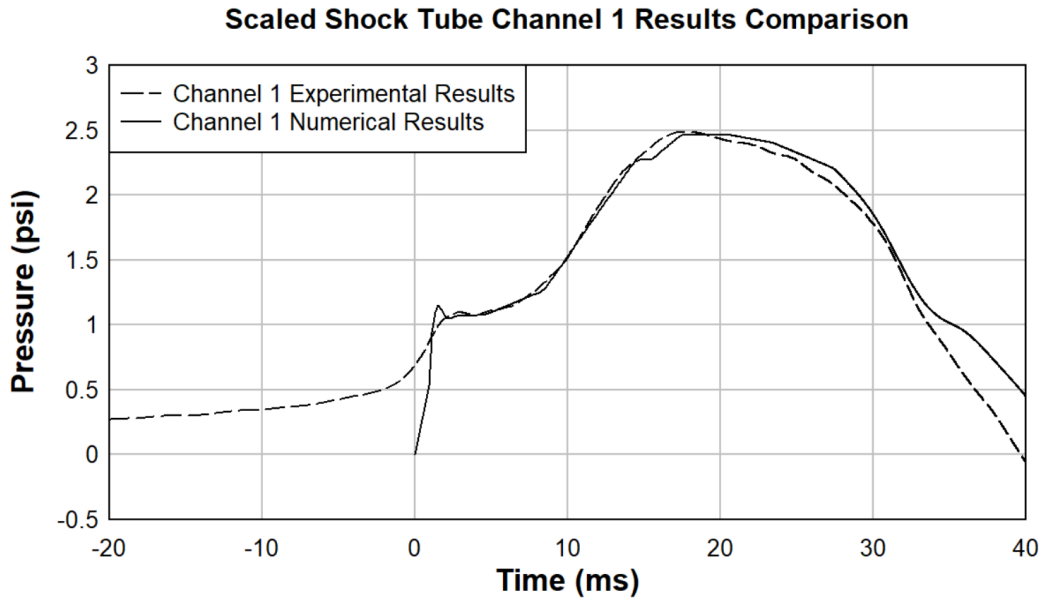

Figure 6-8: Case Study 2 Channel 1 Results Comparison

The pressure vs. time curve for the second pressure sensor location (channel 2) in the scaled shock tube for the total pressure boundary condition model can be seen below in Figure 6-9.

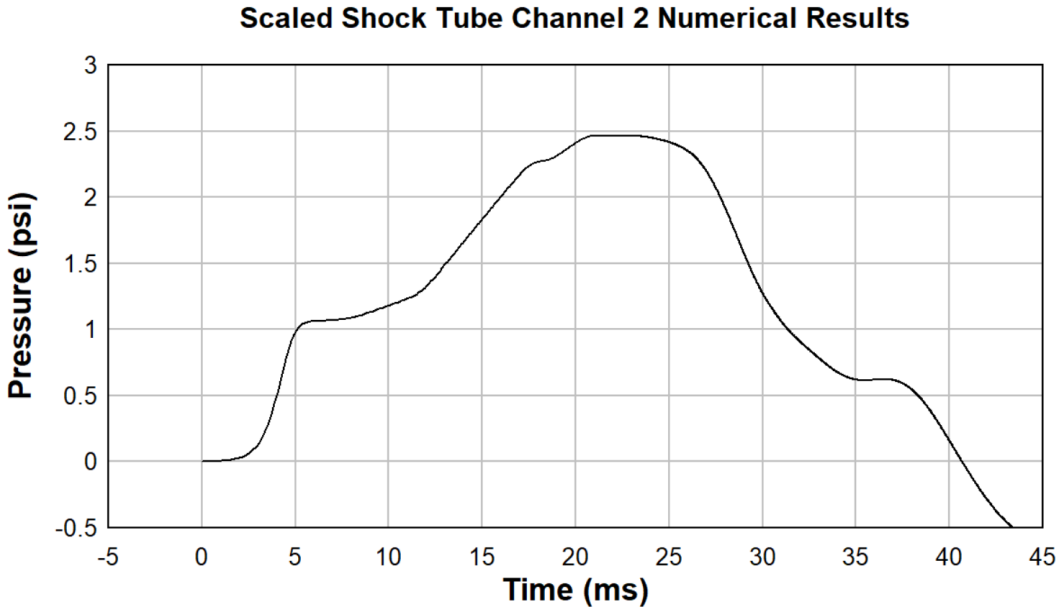

Figure 6-9: Case Study 2 Channel 2 Numerical Results

The numerical results are in excellent agreement with the experimental results. Again, there is not a slow initial pressure rise, as seen in the experimental results, but there are two distinctive pressure rises, an initial one, and one that reaches the peak. Additionally, the duration and shape of the curve is accurate, and no timing adjustment was necessary. The peak pressures are in good agreement. The experimental results reached a peak pressure of 2.40 psi at 19.58 ms, and the numerical results reached a peak pressure of 2.47 psi at 21.34 ms. The comparison of results for case study 2, channel 2, can be seen below in Figure 6-10.

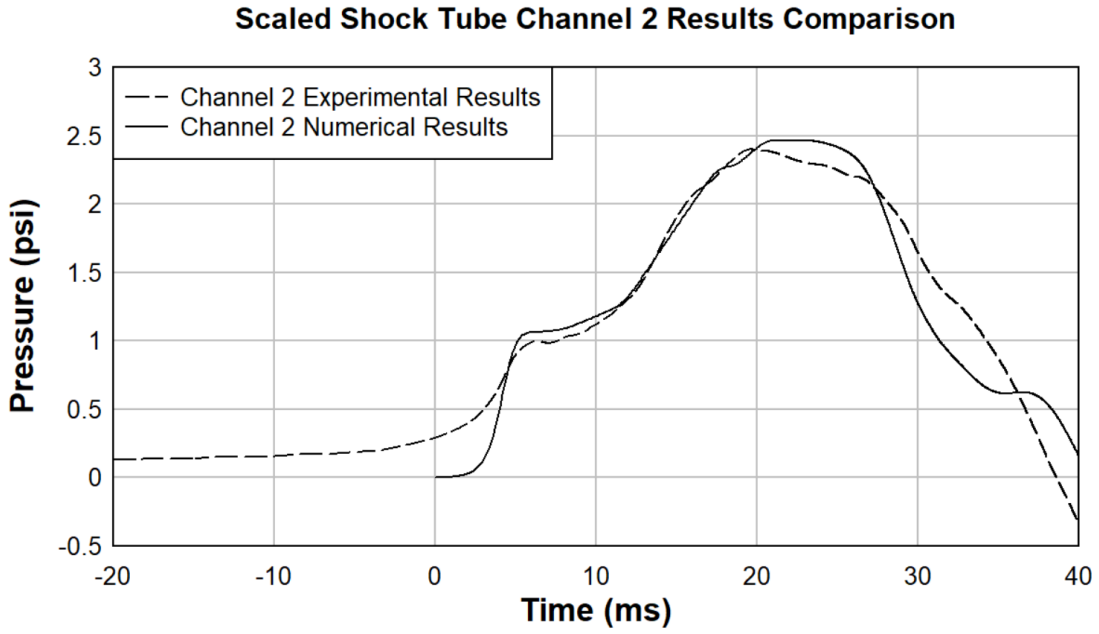

Figure 6-10: Case Study 2 Channel 2 Results Comparison

The pressure vs. time curve for the third pressure sensor location (channel 3) in the scaled shock tube for the total pressure boundary condition model can be seen below in Figure 6-11.

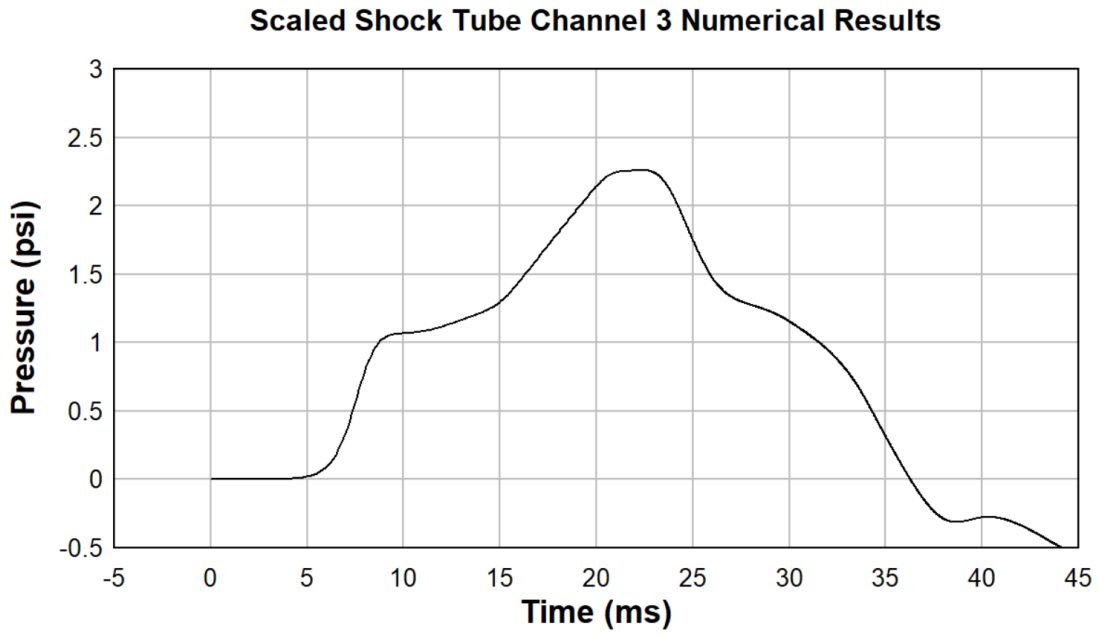

Figure 6-11: Case Study 2 Channel 3 Numerical Results

The numerical results are in excellent agreement with the experimental results. Once again, there is not a slow initial pressure rise, as seen in the experimental results, but there are two distinctive pressure rises, an initial one, and one that reaches the peak. Furthermore, the duration and shape of the curve is accurate, and no timing adjustment was necessary. The peak pressures are in excellent agreement. The experimental results reached a peak pressure of 2.31 psi at 22.51 ms, and the numerical results reached a peak pressure of 2.26 psi at 22.40 ms. The comparison of results for case study 2, channel 3, can be seen below in Figure 6-12.

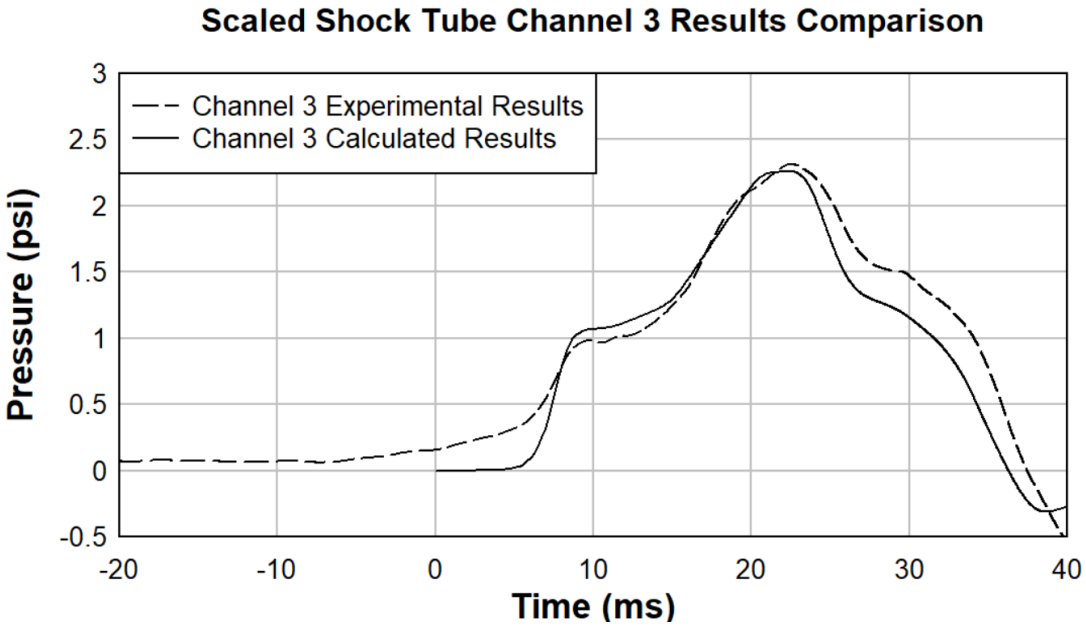

Figure 6-12: Case Study 2 Channel 3 Results Comparison

Case Study 3 Numerical Results

The pressure vs. time curve for the first pressure sensor location (channel 1) in the large shock tube for the bursting balloon model can be seen below in Figure 6-13.

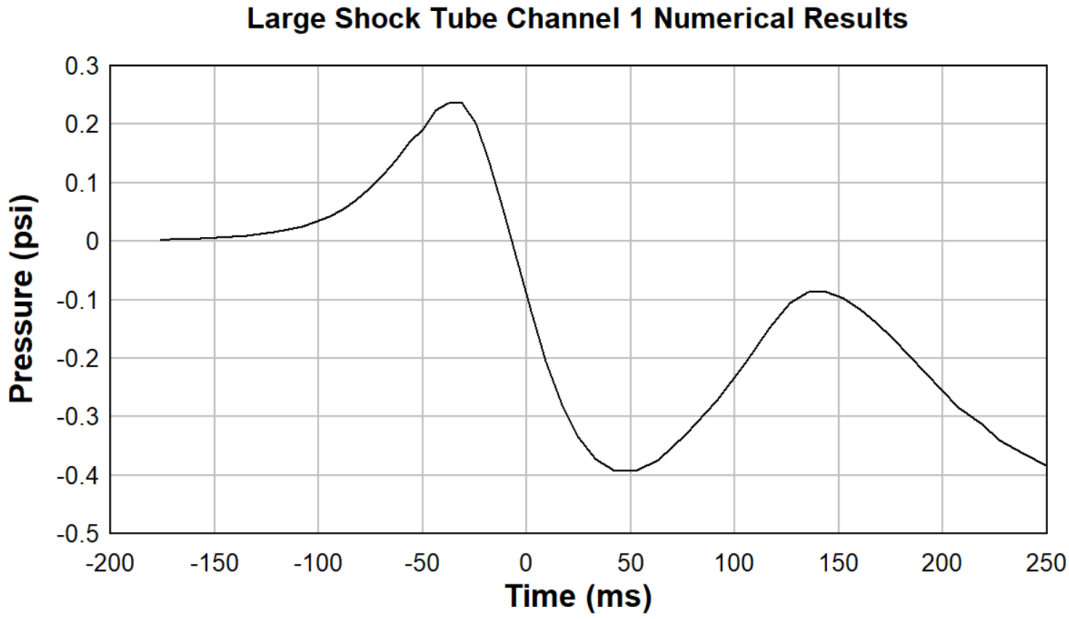

Figure 6-13: Case Study 3 Channel 1 Numerical Results

The timing of the initial pressure rise had to be calibrated with the experimental data. As mentioned previously, the recorded pressure rise can begin before 0 ms, because the timing of the experimental results is solely dependent on the time at which the DataTrap chooses to trigger.

The numerical results are in good agreement with the experimental results. A peak pressure is reached, followed by a negative peak pressure of a slightly higher magnitude, and a subsequent pressure rise to about -0.1 psi. This can be attributed to the suction or negative pressure created by the blast wave, immediately following the positive wave. The experimental and numerical results both exhibit this phenomenon.

Again, there is no distinguished initial pressure rise prior to the pressure rise that reaches the peak. This could be because the model does not account for the membrane burst. The pressure peaks are in good agreement. The experimental results reached a peak pressure of 0.239 psi at -31.53 ms, and the numerical results reached a peak pressure of 0.237 psi at -26.27 ms. The comparison of results for case study 3, channel 1, can be seen below in Figure 6-14.

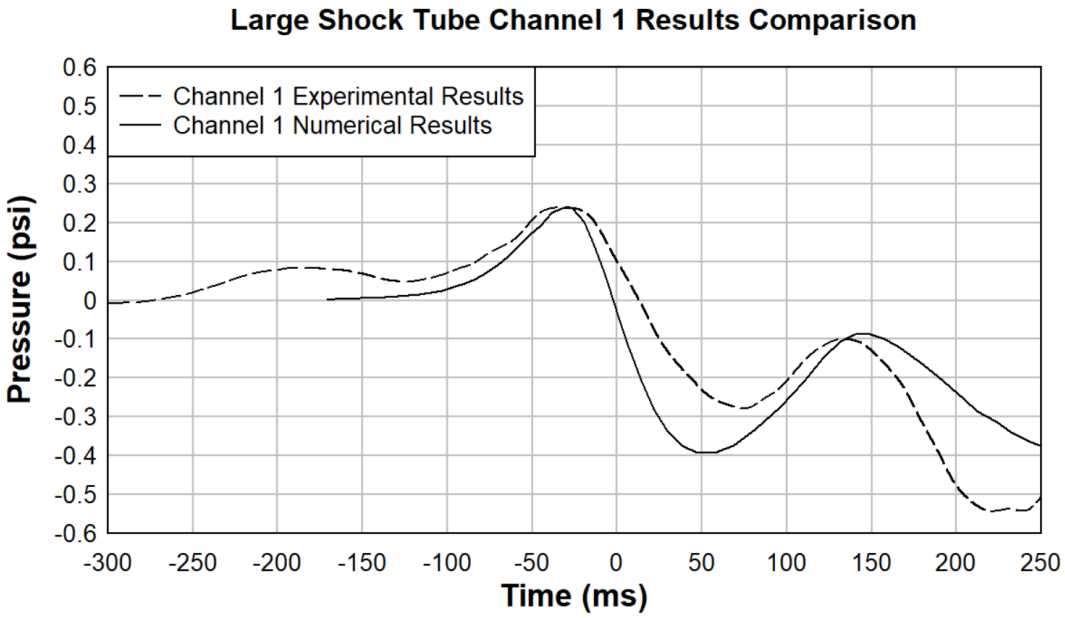

Figure 6-14: Case Study 3 Channel 1 Results Comparison

The pressure vs. time curve for the second pressure sensor location (channel 2) in the large shock tube for the bursting balloon model can be seen below in Figure 6-15.

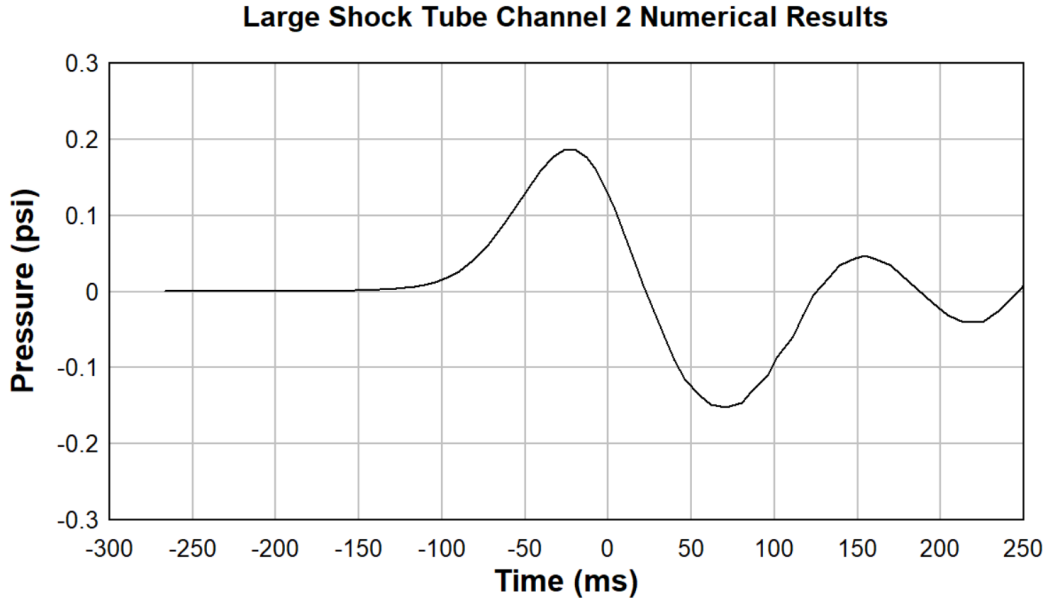

Figure 6-15: Case Study 3 Channel 2 Numerical Results

The numerical results are in good agreement with the experimental results. A peak pressure is reached, followed by a negative peak pressure of a slightly higher magnitude, and a subsequent pressure rise to about 0.18 psi. However, the numerical data has a subsequent pressure rise to only about 0.05 psi.

Once again, there is no distinguished initial pressure rise prior to the pressure rise that reaches the peak. The initial peak pressures are in good agreement. The experimental results reached a peak pressure of 0.212 psi at -17.99 ms, and the numerical results reached a peak pressure of 0.187 psi at –25.82 ms. The comparison of results for case study 3, channel 2, can be seen below in Figure 6-16.

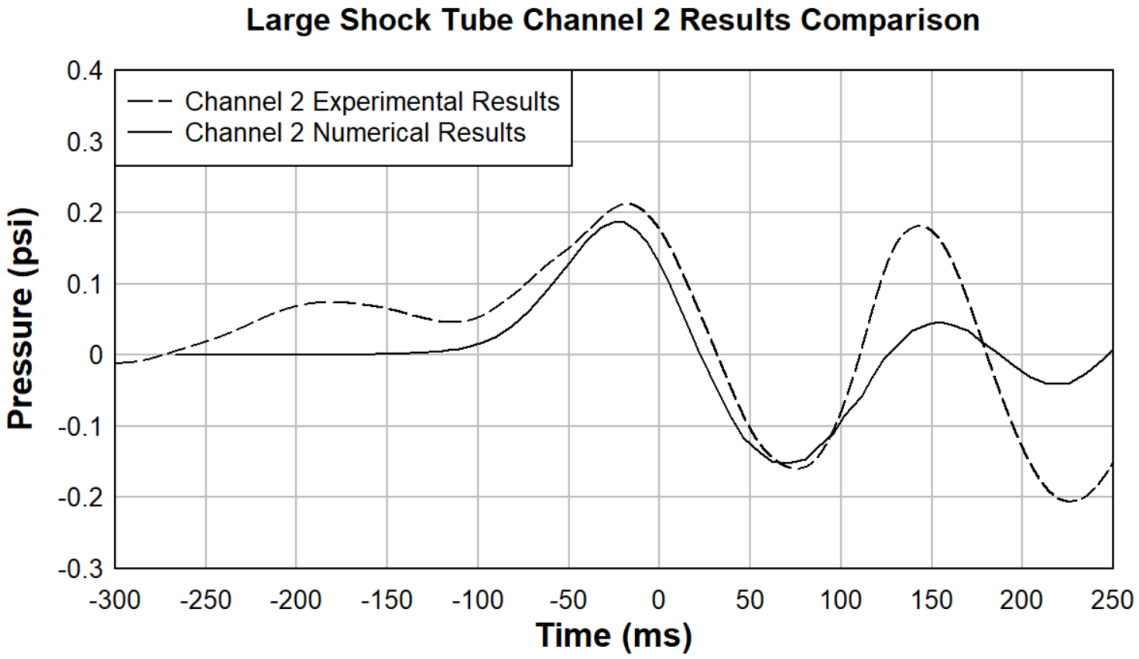

Figure 6-16: Case Study 3 Channel 2 Results Comparison

Results Summary

The first case study, which modeled the combustion of methane in the scaled shock tube, had results that were in good agreement with the experimental data. While the pressure vs. time curves for the numerical data were not complete due to run-time limitations, the peak pressures were reached. This was determined to be sufficient data for comparison of the model at this time. Figure 6-17 below displays all the experimental and numerical pressure vs. time curves for the first case study.

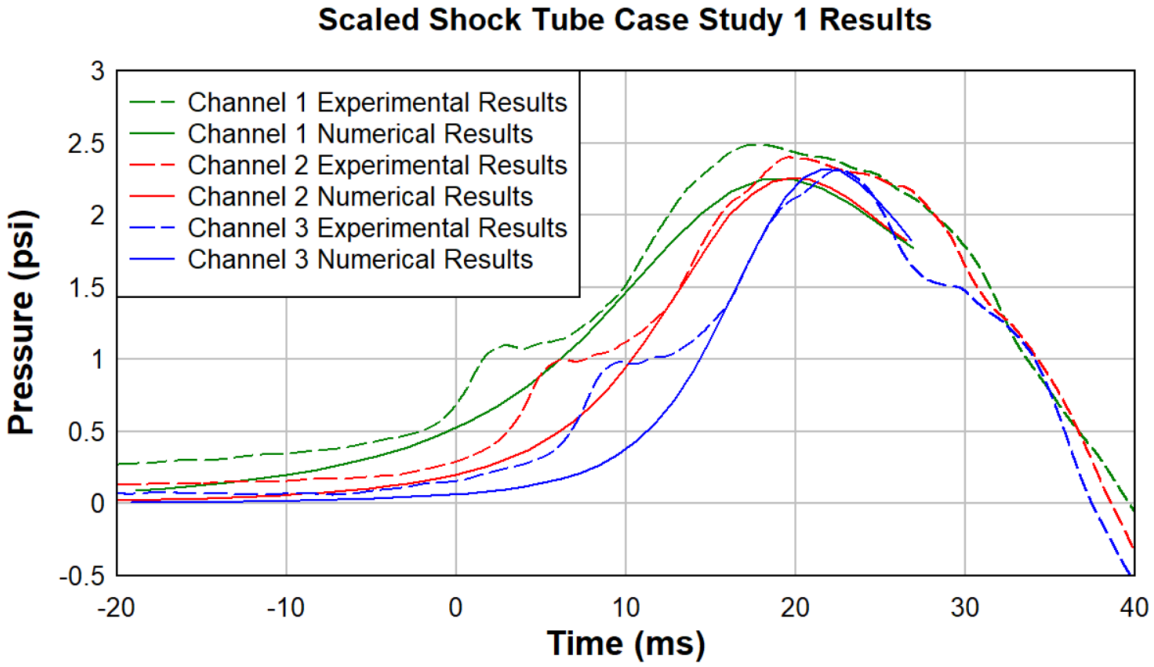

Figure 6-17: Case Study 1 Results Comparison

The second case study, which utilized the total pressure boundary condition to model the scaled shock tube, had results that were in excellent agreement with the experimental data. This can be attributed to the table input feature which allowed a pressure vs. time curve to be assigned to the total pressure boundary, which was at the location of the membrane. Additionally, the durations of the curves were accurate, and no time

adjustment was required. Figure 6-18 below displays all the experimental and numerical pressure vs. time curves for the second case study.

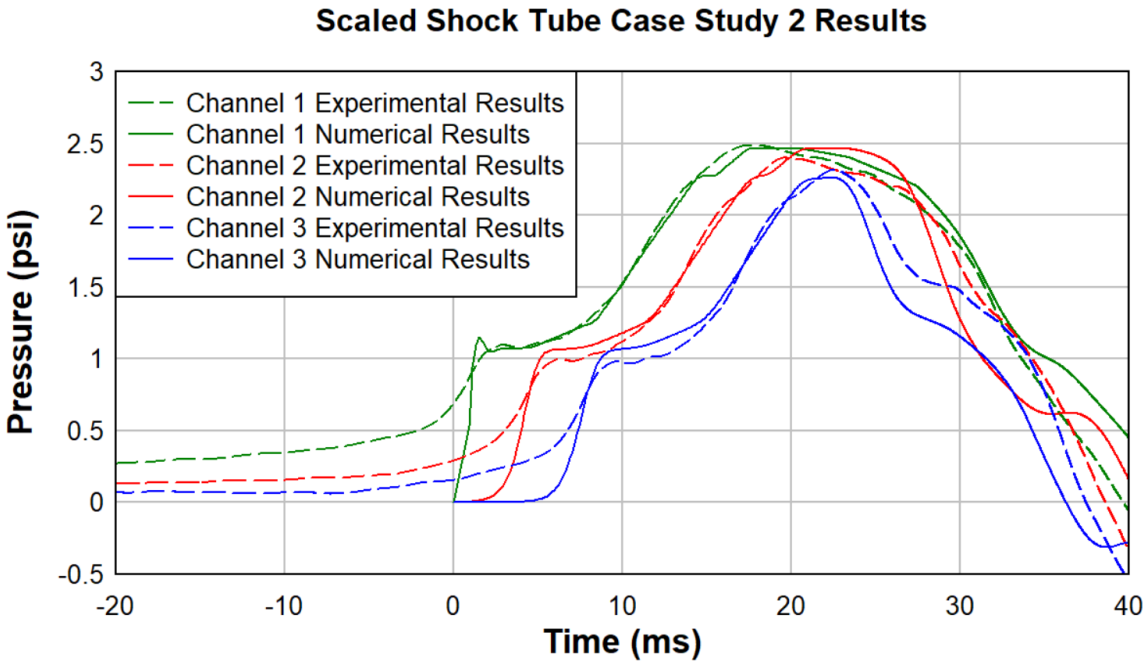

Figure 6-18: Case Study 2 Results Comparison

Finally, the third case study, which utilized the bursting balloon technique to model the large shock tube, had results that were in good agreement with the experimental data. For the first pressure sensor (channel 1), the initial and subsequent peak pressures were similar in magnitude. For the second pressure sensor (channel 2), the initial peak pressure was also similar in magnitude, however, the subsequent peak pressure was not. Also, a negative pressure impulse was experienced between the two pressure peaks for both sensors, which could be attributed to the suction or negative pressure created by the blast wave, immediately following the positive wave. Figure 6-19 below displays all the experimental and numerical pressure vs. time curves for the third case study.

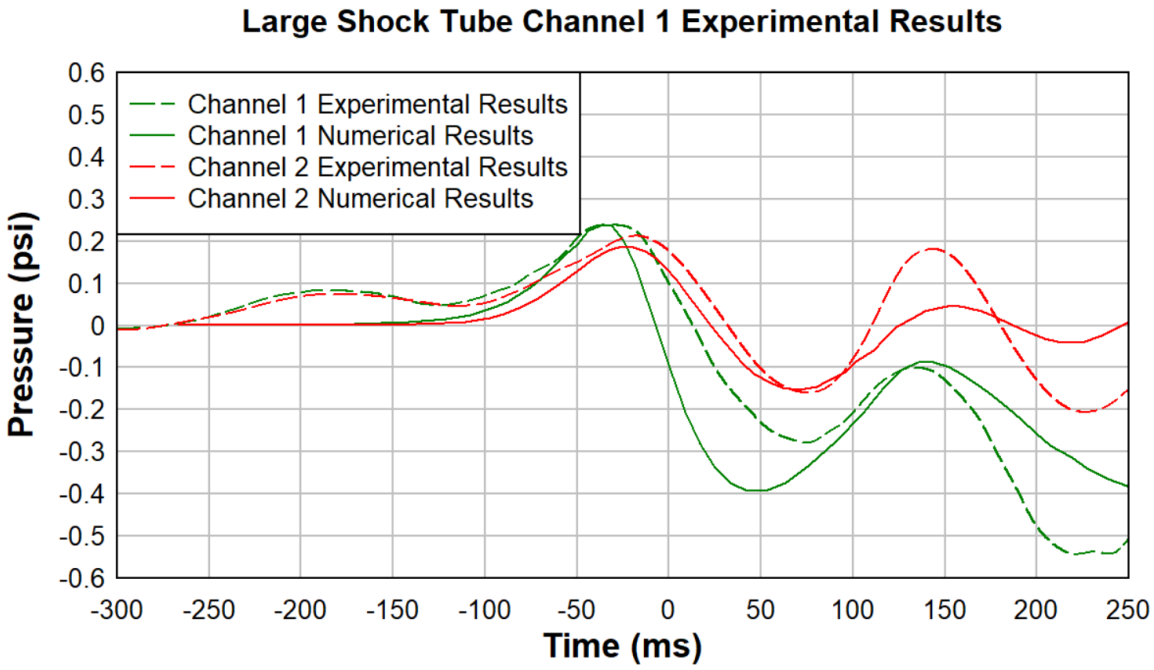

Figure 6-19: Case Study 3 Results Comparison

CHAPTER 7. CONCLUSIONS AND FUTURE WORK

Chapter 7 discusses the conclusions drawn from the research conducted for this thesis. It also includes recommendations for future work that can be conducted to continue the improvement of modeling explosions. Below, Table 7-1 provides a comparison of the three modeling methods employed to model methane explosions.

Table 7-1: Modeling Techniques Comparison

Method	Model Dimensions	Mesh Size (Elements)	Peak Pressure Percent Differences	Run Time
Chemical Reactions (Combustion of Methane)	0.4" x 11" x 11.5'	501,181	Ch 1: 10.1% Ch 2: 6.0% Ch 3: 0.4%	16 hrs
Total Pressure Boundary Condition	10.875" x 11" x 18'	598,897	Ch 1: 0.8% Ch 2: 2.9% Ch 3: 2.2%	40 min
Bursting Balloon	8' x 8' x 13.5'	180,256	Ch 1: 0.8% Ch 2: 12.5%	20 min

Conclusions

Methane and coal dust explosions continue to be the most significant hazard in underground coal mines. Traditionally, mine explosion data could only be gathered through large scale testing in experimental mines. However, even experimental mine explosions have their limitations in terms of the volume of methane-air mixture that can be ignited. CFD modeling can provide a means for gathering pressure-time history data for larger explosions.

Three case studies were investigated to examine alternatives ways to model methane explosions which allowed for reduced run-times and easier model calibration to experimental data. All case studies used the commercial CFD software, SC/Tetra. The first case study modeled the combustion of methane in a scaled shock tube measuring 10.875 inches by 11 inches by 20.5 feet long. Three Piezotronic dynamic pressure sensors installed

along the roof of the shock tube provided useable experimental data for model validation from a methane explosion with a 2.5-foot-long cloud, at a concentration of 9% methane. The numerical results from the CFD model were in good agreement with the experimental data, with all pressure peaks within 0.25 psi of the recorded pressure data. However, the model had an extensive run-time of 16 hours to reach the peak pressures.

To remedy this issue, the second case study utilized a total pressure boundary condition at the location of the membrane to model the same methane explosion in the scaled shock tube, instead of modeling the combustion of methane. A table input featured allowed a pressure vs. time curve to be assigned to the total pressure boundary, which accurately recreated the pressure profile released from the explosive methane-air mixture. This was made possible with the knowledge of the experimental data. This method provided results that were in excellent agreement with the experimental results. The shape and durations of the curves were accurate, and no time adjustment was required. All numerical pressure peaks were within 0.07 psi of the recorded pressure data. Alternatively, this model had a run-time of approximately 40 minutes. However, this method of modeling required the experimental data of at least one pressure sensor point to appropriately calibrate the model.

Furthermore, the third case study utilized the bursting balloon technique, typically used to model high explosives, to model a methane explosion in a large shock tube. The shock tube measured 8 feet by 8 feet by 40 feet long, and had a 4-foot-long methane cloud, at a concentration of 9% methane. Two Piezotronic dynamic pressure sensors installed in the side of the shock tube provided experimental data for model validation. This simulation did not model the combustion of methane, but instead the equivalent energy release. An

initial pressure condition of 0.36 psi, and an initial velocity condition of 311 ft/s was applied to the methane-air mixture volume of the model. This method provided results that were in good agreement with the experimental results. The experimental data from both pressure sensor locations showed a peak pressure, followed by a negative peak pressure of a slightly higher magnitude, and a subsequent pressure rise. This could be attributed to the suction or negative pressure created by the blast wave, immediately following the positive wave. The numerical results also exhibited this phenomenon. The initial peak pressures of the numerical data were within 0.025 psi of the recorded pressure data. Additionally, this model had a run-time of approximately 20 minutes.

The results of this research provided validation that there are alternative ways to successfully model methane explosions, without having to model the chemical reactions involved in the combustion of methane. Modeling these chemical reactions required a smaller mesh, and a subsequent longer run-time. Relatively accurate results were achieved utilizing the total pressure boundary condition, and the bursting balloon technique. These models had run-times of approximately 40 minutes and 20 minutes respectively. Additionally, these models were easily calibrated to experimental data through changing the pressure vs. time curve for the total pressure boundary condition, or increasing/decreasing the initial pressure and velocity assigned to the methane-air mixture volume. Continued research in this field to investigate the application of these methods to larger scale explosions would further prove their validation as accurate methods of modeling.

Future Work

This research provided validation for the use of alternative methods to model methane explosions on a relatively small scale. These methods should be applied to larger scale explosion events to determine their accuracy and their ability to model explosions more quickly than traditional methods (modeling the combustion of methane). This research was limited to the UKERT test facilities, the scaled shock tube and the large shock tube. Neither of these testing environments allowed for the continued propagation of a methane explosion, where the explosion could transition from deflagration to detonation. Additionally, validation of this research in proper mine geometry with entries and cross-cuts should be investigated.

Case Study 1 S File

```
SDAT
SC/Tetra
  13   0   0     UTF-8
PREI    test_combustion.pre
RO      test_combustion.r
POST    test_combustion
TM      test_combustion.csv
/
   1   1   0

  10   1
CHKL
                1                   1                   0                   1                   0
CYCL
      1    2000               1e-006       1                   1
EQUA
11111111111111
FLUX
%CNAM Flux_1
   0   2   0   1   0   1
                 29   0
               26.85
               0.121               0.208                   0               0.671                   0
                  0                   0                   0                   0                   0
fuel_in
/
%CNAM Flux_2
 -14   0   1   0   0   0
                  0
out
/
/
GFIL
                 50   1
GRAV
                  0                -9.8                   0
GWLN
   0
INIT
PRES
                  0   0
/
```

```
INIT
TEMP
              26.85   0
/
INIT
CN01
              0.095  -1
v_nozzle
/
                0  -1
v_fire
/
                0  -1
v_cbr
/
/
INIT
CN02
                0  -1
v_nozzle
/
                0  -1
v_fire
/
             0.23184  -1
v_cbr
/
/
INIT
CN03
                0  -1
v_nozzle
/
              0.01  -1
v_fire
/
                0  -1
v_cbr
/
/
INIT
CN04
              0.905  -1
v_nozzle
/
              0.99  -1
```

```
v_fire
/
            0.76816  -1
v_cbr
/
/
LOOP
  10
PCTY
  4
PROP
%CNAM ‹ó‹C(”ñˆ³□k20□Ž)
  1   3            8.31451              -1              -1              -1   1
/
                0          -4667020          0.016       5.02e-005          5830
0.415
                0                0          0.032       8.91e-005          1228
0.153
                0         -13434778          0.018       8.26e-005          2933
0.352
                0                0          0.028         7.5e-005         1286
0.136
                0          -8941853          0.044       7.63e-005          1363
0.145
                0          15574290          0.016       9.33e-005          1315
0.182
                0          33746710          0.014       9.32e-005          1560
0.207
                0           3009128           0.03       8.19e-005          1219
0.139
                0           2289469          0.017       8.09e-005          2104
0.243
                0         216268800          0.001       3.16e-005         18228
0.977
REAC
  1   0
                1   1              1
                2   2              2
/
                2   3
                1   5
/
               -2              1              0
  0
                1   4              1
                1   6              1
```

/
1 8
1 7
/
180000000 0 38370
0
1 8 1
1 7 1
/
1 4
1 6
/
38000000 0 425
0
1 7 1
1 2 1
/
1 8
1 6
/
18000 1 4680
0
1 8 1
1 6 1
/
1 7
1 2
/
3800 1 20820
0
1 7 1
1 9 1
/
1 8
1 10
/
71000000 0 450
0
1 8 1
1 10 1
/
1 7
1 9
/
170000000 0 24560
0

```
/
SDIF
  2   1
              3.746              141                0
              3.458            107.4                0
              2.605            572.4            1.217
              3.621            97.53                0
              3.763              244                0
               2.75               80                0
              3.298             71.4                0
              3.621            97.53                0
               2.75               80                0
               2.05              145                0
SNAM
ch4
o2
h20
n2
co2
o
n
no
oh
h
SOLV
   1   5 100              1e-006
   2   5 100              1e-006
   3   5 100              1e-006
   4   8 500              1e-006
   5   5 500              1e-006
   6   5 100              1e-006
   7   5 100              1e-006
   8   5 200              1e-006
   9   5 200              1e-006
  10   5 200              1e-006
  11   5 200              1e-006
  12   5 200              1e-006
  13   5 200              1e-006
  14   5 200              1e-006
  15   5 200              1e-006
  16   5 200              1e-006
  17   5 200              1e-006
/
STBT
   1
TMSR
```

```
Point_1          0.005          0.266          0.9144   0   0          1   0
PRES
/
Point_2          0.005          0.266          2.1336   0   0          1   0
PRES
/
Point_3          0.005          0.266          3.3528   0   0          1   0
PRES
/
/
TRAN
  1
WL02
%CNAM Wl02_1
  0   0
/
  1
wall
/
/
WL04
%CNAM Wl04_1
                0   0              0   0
wall
/
/
WPUT
  0
ZGWV
  0
GOGO
```

Case Study 2 S File

```
SDAT
SC/Tetra
  13   0   0     UTF-8
PREI    total_pressure_boundary.pre
RO      total_pressure_boundary.2.r
POST    total_pressure_boundary
TM      total_pressure_boundary.csv  A
/
   1   1   0

   0   1
CHKL
                  1                  1                  0                  1                  0
CMDS
Table_1
TTYP
TIME
VTBL
                  0               7600
              0.004               7600
              0.008               9000
              0.014              16500
              0.015              16500
              0.017              18000
               0.02              18000
              0.023              17500
              0.027              16000
              0.045                  0
/
ENDT
CMDE
CYCL
      1    1300              1e-005       1                  1
EQUA
1111
FLUX
%CNAM Flux_1
  -4   0   1   0   0   0
                  0
outlet
/
%CNAM Flux_2
  -2   0   1   0   0   0
```

```
          "@S:Table_1"
membrane
/
/
GFIL
                50   0
INIT
TEMP
              26.85  -1
tube_air
/
/
PROP
%CNAM air(compressible/20C)
  1   3              287.06            1.83e-005              1007              0.0256   0
/
TMSR
Point_1           0.1381125              0.279            0.1524    0    0              1    0
PRES
/
Point_2           0.1381125              0.279            1.3716    0    0              1    0
PRES
/
Point_3           0.1381125              0.279            2.5908    0    0              1    0
PRES
/
/
WL02
%CNAM Wl02_1
  9   0
/
  1
walls
/
/
WL04
%CNAM Wl04_1
                0   0                  0   0
walls
/
/
GOGO
```

Case Study 3 S File

```
SDAT
SC/Tetra
  13   0   0 UTF-8
PREI    bursting_balloon.pre
RI      bursting_balloon.r
RO      bursting_balloon.2.r
POST    bursting_balloon
TM      bursting_balloon.csv  A
/
   1   1   0

   0   1
BASI
   0              101325                 0                 0
/
CHKL
                  1                 1                 0                 1                 0
CYCL
      1     200              0.001       1             1
EQUA
1111
FLUX
%CNAM Flux_1
  -4   0   0   0   0   0
outlet
/
/
GFIL
                 50   0
INIT
VELY
                 95  -1
methane_air_mixture
/
/
INIT
PRES
                  0  -1
tube_air
/
                2500  -1
methane_air_mixture
/
/
INIT
```

```
TEMP
                474  -1
methane_air_mixture
/
                298  -1
tube_air
/
/
PROP
%CNAM air(compressible/20C)
  1   3              287.06            1.83e-005              1007              0.0256   0
/
TMSR
Point_1              1.219              1.2192             2.4384    0    0                1    0
PRES
/
Point_2              1.219              1.2192             3.9624    0    0                1    0
PRES
/
/
WL02
%CNAM Wl02_1
  9   0
/
  1
walls
/
/
WL04
%CNAM Wl04_1
                 0   0                  0   0
walls
/
/
GOGO
```

REFERENCES

Brune, J. F., Cashdollar, K. L., & Zipf, R. K. (2007). *Explosion Prevention in United Sates Coal Mines.* NIOSH, Centers for Disease Control and Prevention. Retrieved from https://www.cdc.gov/niosh/mining/UserFiles/works/pdfs/epius.pdf

Cashdollar, K. L., Zlochower, I. A., Green, G. M., Thomas, R. A., & Hertzberg, M. (2000). Flammability of Methane, Propane, and Hydrogen Gases. *Journal of Loss Prevention in the Process Industries*, 327-340.

Davis, S. G., Engel, D., & Wingerden, K. v. (2015). Complex Explosion Development in Mines: Case Study - 2010 Upper Big Branch Mine Explosion. *Process Safety Progress, 34*(3), 286-303.

Diaz-Ovalle, C., Lopez-Molina, A., & Vazquez-Roman, R. (2016). A CFD-based Approach to Predict Explosion Overpressure: A Comparison to Current Methods. *Chem. Biochem. Eng. Q.*, 419-427.

Fuels and Chemicals - Auto Ignition Temperature. (2003). Retrieved from The Engineering ToolBox: https://www.engineeringtoolbox.com/fuels-ignition-temperatures-d_171.html

Hartmann, I. (1954). Dust Explosions in Coal Mines and Industry. *The Scientific Monthly, 79*(2), 97-108.

Kissell, F. N., Tien, J. C., & Thimons, E. D. (2007). *Methods for Controlling Explosion Risk at Coal Mine Working Faces.* NIOSH, Centers for Disease Control and Prevention. Retrieved from https://www.cdc.gov/niosh/mining/UserFiles/works/pdfs/mfcer.pdf

Kozubkova, M., Krutil, J., & Nevrly, V. (2014). Experiments and Mathematical Models of Methane Flames and Explosions in a Complex Geometry. *Combustion, Explosions, and Shock Waves, 50*(4), 374-380.

Kruger, R. A., Plessis, J. J., & Vassard, P. S. (1996). *The Potential of Fly Ash for the Control of Underground Coal Dust Explosions.* CSIR Division of Mining Technology.

Laundry, B. E., & Sharma, B. I. (1974). Application of the Energy-Dissipation Model of Turbulence to the Calculation of Flow Near Spinning Disc. *Letters in Heat and Mass Transfer, 1*(2), 131-137. Retrieved from https://www.sciencedirect.com/science/article/pii/0094454874901507?via%3Dihub

Light, T. E., Herndon, R. C., & Guley, A. R. (2007). *Report of Investigation: Fatal Underground Coal Mine Explosion May 20, 2006.* Mine Safety and Health

Administration, United States Department of Labor. Retrieved from https://arlweb.msha.gov/FATALS/2006/Darby/FTL06c2731.pdf

McActeer, J. D. (2006). *The Sago Mine Disaster, A Preliminary Report to Governor Joe Manchin III.* Retrieved from http://www.wju.edu/sago/SagoMineDisasterReport_July2006.pdf

McMahon, G. W., Britt, J. R., & Walker, R. E. (2010). Methane Explosion Modeling in the Sago Mine. *Mining Engineering*, 51-62.

MSHA. (2007). *Sago Mine Information.* Mine Safety and Health Administration, United States Department of Labor. Retrieved from https://arlweb.msha.gov/sagomine/sagomine.asp

O'Brien, G. (2011). *Culture Kills - The Legacy of Massey Energy*. Retrieved from The Week in Ethics: https://theweekinethics.wordpress.com/tag/upper-big-branch-mine-explosion/

Solomos, G., Casadei, F., Giannopoulos, G., & Larcher, M. (2011). *Experimental and Numerical Simulation Activities for the Assessment of Explosion Effects in a Train Station.*

WVMHS&T. (2011). *Upper Big Branch Mine Disaster Investigative Report Summary.* West Virginia Office of Miner's Health, Safety and Training. Retrieved from http://www.wvminesafety.org/PDFs/Performance/EXECUTIVE%20SUMMARY.pdf

Xu, G., Luxbacher, K. D., Ragab, S., Xu, J., & Ding, X. (2016). Computational Fluid Dynamics Applied to Mining Engineering: A Review. *International Journal of Mining, Reclamation and Environment*, 251-275.

Yonts, B. (2018). *Analysis of Underground Coal Mine Structures Subjected to Dynamic Events.* University of Kentucky.

Zipf, R. K., Sapko, M. J., & Brune, J. F. (2007). *Explosion Pressure Design Criteria for New Seals in U.S. Coal Mines.* NIOSH, Centers for Disease Control and Prevention. Retrieved from https://www.cdc.gov/niosh/mining/UserFiles/works/pdfs/2007-144.pdf

VITA

Laura Steeves

Education

Master of Science in Mining Engineering at the University of Kentucky, August 2017-present. Thesis title: "Simplifying Techniques Applied to Computational Fluid Dynamics Modeling of Methane Explosions."

Bachelor of Science (May 2017) in Mining Engineering, University of Kentucky, Lexington, Kentucky.

Academic Employment

Graduate Research Assistant to Dr. Jhon Silva, Department of Mining Engineering, University of Kentucky, May 2017-present.

Undergraduate Research Assistant to Dr. Chad Wedding, Department of Mining Engineering, University of Kentucky, May 2016-August 2016.

Scholastic and Professional Honors

Henry DeWitt Smith Graduate Scholarship 2018

Margaret Ingles SWE Graduate Fellowship 2017

WAAIME Scholarship 2017

Mu Nu Gamma (MNG) Honor Society Induction 2016

Professional Publications

Spaeth, A., Steeves, L., Silva, J., & Perera, I. E. (2019). Overview of Active Explosion Barrier Systems for Underground Coal Mines. 17th North American Mine Ventilation Symposium.